

Coseismic crustal deformation on a fault zone defined by microseismicity in the Pavliani area, central Greece

Paul W. Burton,^{1,*} Nikolaos S. Melis^{2†} and Mike Brooks²

¹*School of Environmental Sciences, University of East Anglia, Norwich NR4 7TJ, UK*

²*Department of Geology, University of Wales College of Cardiff, P.O. Box 914, Cardiff CF1 3YE, UK*

Accepted 1995 April 21. Received 1994 December 5; in original form 1994 January 10

SUMMARY

Pavliani is an area of high microseismicity in northern central Greece. There is no evidence in the historical record of large damaging earthquakes in this area since at least 600 BC. We examine contemporary crustal deformation in this area using microearthquake data recorded during 1983–84 by the Volos seismic network, principally, and to a lesser extent by the Patras seismic network.

The microseismicity (1–4.6 M_L) defines an approximately vertical fault zone trending WSW–ENE, of 55 km length and 25 km depth. The fault-plane solution for the 4.6 M_L earthquake shows a strike consistent with the trend of the microseismicity zone, and an extension direction consistent with many large earthquakes in central Greece associated with the extensional greater Aegean. Spectra of the microearthquakes are estimated using P waves obtained by selective windowing designed to exclude other P phases from the coda; seismic moments in the range $1–95 \times 10^{12}$ N m are obtained, accompanied by estimates of seismotectonic source parameters, including source radii, average stress drop and average coseismic slip. Of prime utility is an excellent correlation found between seismic moment and magnitude, and with coseismic slip. This allows heterogeneity in the distribution of individual microearthquake source parameters to be mapped onto the vertical fault-zone plane and the history of coseismic deformation for the whole seismicity observed during 1983–84 to be examined using cumulative slip and moment-release rate. Peaks of high moment-release rate occur in the east and centre of the fault zone. That in the east is dominated by a few large moment-release events; that in the centre by a large number of small events. Both moment-release-rate peaks, despite their different component seismicity, are associated with high cumulative coseismic slip. Only the eastern peak is also associated with high stress drop; it is also shallower, and therefore any surficial interaction is less likely to be attenuated. The surface projection of this peak is within 3 km of a mapped normal fault coincident with an Alpine thrust front delineated by a major scarp of Mesozoic limestone. Surface evidence of recent movement on this normal fault is only slight. Friable fault gouge is seen at a few localities. Displacement could not be determined because the limestone surfaces are deeply weathered and lack kinematic indicators. However, considering the whole fault zone as a cohesive entity, and using a Brune estimate of slip at the current moment-release rate throughout the present extensional tectonic regime, suggests a total vertical displacement of order 175 m, similar to the elevation of the scarp.

Key words: crustal deformation, Greece, microearthquakes, tectonics.

* Address for correspondence: P. W. Burton, School of Environmental Sciences, University of East Anglia, Norwich NR4 7TJ.

† Now at: 89A Asimakis Fotilas Street, GR-262 24, Patras, Greece.

1 INTRODUCTION TO THE PAVLIANI AREA

Overall seismicity amidst the tectonic complexities that form the seismotectonics of Greece is broadly reviewed in detail by Bath (1983). The study area of Pavliani lies in the northern part of central mainland Greece, within a mountain chain consisting of the Kallidromon, Giona, Vardousia and Oiti Mountains (Fig. 1) which form part of the major Hellenide orogenic belt of Alpine age. The Pavliani area is surrounded by major neotectonic features indicative of an active extensional regime. For example: the Spercheios River graben to the north, which extends eastwards to the Gulf of Maliakos, the normal fault zone of Atalandi to the east, and the Gulf of the Corinth graben to the south, which Melis, Brooks & Pearce (1989) suggested extends westwards to Trikhonis Lake (Fig. 1). Focal mechanisms of large shallow events that

have occurred over the last 30 years indicate approximately N–S extension for these regions (Ritsema 1974; Papazachos 1976; McKenzie 1978; Drakopoulos & Delibasis 1982; Papazachos *et al.* 1984; Papadopoulos *et al.* 1986; Melis *et al.* 1989). At a local scale, faulting of WSW–ENE (260°) trend has been mapped at 1:50 000 (IGME 1960), and related topographic features have been observed south of the village of Kaloscopi on 1:30 000 aerial photographs. This faulting suggests active tectonism in the area for which no previous studies exist.

During 1983–84 there was extensive microearthquake activity near Pavliani. In this paper, we examine the seismicity of the Pavliani area, particularly the microseismicity, and its potential contribution to coseismic crustal deformation. The zone of crustal deformation is shown to be tightly constrained spatially and its possible relationship with surface geological features is explored.

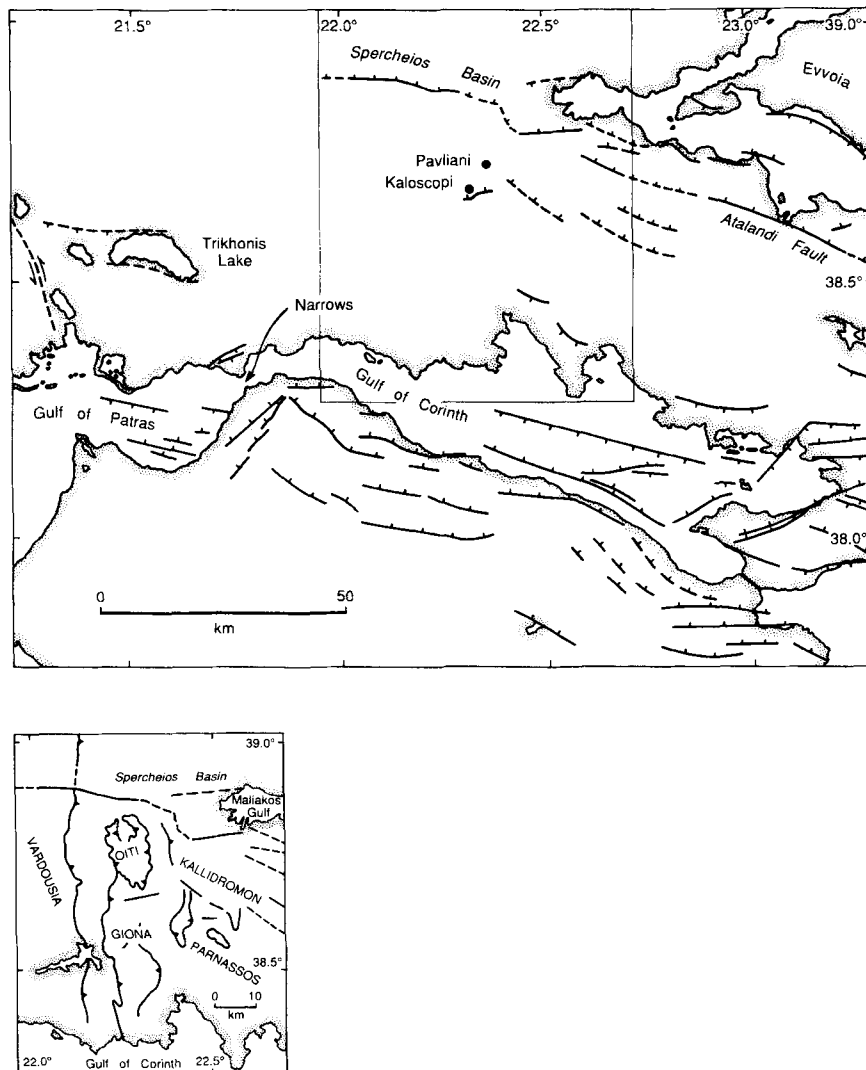


Figure 1. Summary of the regional system of neotectonics in the major area of central Greece (after Brooks & Ferentinos 1984; Ferentinos *et al.* 1985; Vita-Finzi & King 1985; King *et al.* 1985; Brooks *et al.* 1988, Doutsos & Piper 1990; Collier & Dart 1991; Roberts & Jackson 1991). The smaller window is extracted as a location map of the Pavliani area and shows major Alpine and neotectonic structures of this region with thrusts identified by teeth on the overthrust side of the fault.

2 SEISMICITY IN PAVLIANI

2.1 Historical seismicity

Earthquake catalogues available for Greece for the years 1900 to 1985 (Comninakis & Papazachos 1986; Makropoulos & Burton 1981; Makropoulos, Drakopoulos & Latousakis 1989) show that 17 earthquakes of surface-wave magnitude (M_s) between 4.0 and 5.2 (Table 1) have occurred within or near to the area of Pavliani (Fig. 2). There have been no large destructive earthquakes during this period. The Galanopoulos (1960, 1961, 1981) and Papazachos & Papazachos (1989) catalogues of historical seismicity prior to 1900 show that no large earthquakes are known to have occurred in the area since at least 600 BC, a result in agreement with Ambraseys & Jackson's (1990) study of historical seismicity in Greece. Table 1 shows that 10 of the 17 earthquakes are shallow, with focal depths between 5 and 33 km, and surface-wave magnitude between 4.0 and 4.8 M_s .

2.2 Microseismicity

Two microearthquake networks operated contemporaneously in central Greece during 1983–84, namely VOLNET (Volos Seismic Network, Monthly Bulletins; Burton *et al.* 1983–84) and PATNET (Patras Seismic Network; Melis 1986). Table 2 gives details of all station locations. VOLNET is a large network with an aperture of 100 km (Fig. 3), and was designed to investigate the seismic activity in eastern central Greece as well as coordinating with the main Greek National Network to produce more accurate locations for events occurring in the larger mainland area of Greece (Burton *et al.* 1991). PATNET

has a 40 km aperture (Fig. 3). It was designed principally to examine seismicity in the Gulf of Patras and is associated with the Rio-Antirrio Narrows (Melis *et al.* 1989). Both networks utilized Willmore MkIII seismometers which operate as velocity transducers. VOLNET seismometers were calibrated at 1.5 s natural period, PATNET at 1.0 s, and both at 0.7 damping. This short-period instrument has an appropriate spectral window to view the frequencies in the microearthquakes examined.

In what follows, greater prominence is given to the data from the Volos Network, which includes a telemetered station at Pavliani, except when *P*-wave first-motion data are used to discuss the 4.6 M_L earthquake of 1983 September 19.

Magnitudes determined from the Volos network adopt the standard Richter procedure (Richter 1958), using either horizontal (hence M_{LH}) or vertical (hence M_{LV}) components. Both M_{LH} and M_{LV} have been correlated with local magnitudes given by the Athens National Observatory to obtain standard magnitude corrections (Burton *et al.* 1991). These corrections are used in the present study to convert M_{LV} to a standard local magnitude compatible with the Athens National Observatory local magnitudes. This is the common base for both networks (PATNET magnitudes derive in the first instance from duration magnitude but are also corrected to M_L Athens).

A few earthquakes were recorded by the Patras network as well as by the Volos network. For these common events, which occurred during the 1983 July–1984 January period of overlapping recordings, there are differences between the locations computed using PATNET records only, VOLNET records only, and PATNET–VOLNET combined records. These differences are discussed in detail by Melis (1992), who shows

Table 1. Earthquake parameters for the period 1900–85.

Origin Time (year mon day hr min sec)	Latitude (°N)	Longitude (°E)	Depth (km)	Magnitude (M_s)	Number of stations or catalogue id.
1914 Mar 23 5 9 16.0	38.60	22.30	33	4.2	PC
1931 Apr 30 18 10 50.0	38.60	22.50	33	4.7	PC
1931 Dec 6 5 24 40.0	38.60	22.00	33	4.6	UNS
1960 Jun 2 4 25 10.0	38.70	22.30	5	4.0	UNS
1939 Jun 2 14 11 43.0	38.65	22.09	148	5.2	18
1949 Oct 4 17 33 33.9	38.63	22.08	111	5.0	31
1957 Nov 9 23 55 58.5	38.57	22.54	23	4.8	42
1964 Dec 1 10 21 3.3	38.53	22.45	48	4.7	15
1965 Jan 10 8 2 51.7	38.70	22.00	46	4.3	18
1970 May 8 18 30 42.7	38.67	22.30	58	4.4	70
1976 Jun 5 20 30 11.5	38.58	22.21	51	4.0	16
1976 Jun 20 4 51 17.0	38.53	22.12	51	4.7	17
1979 Nov 27 10 27 17.7	38.77	22.00	10	4.0	26
1982 Jul 17 18 24 55.2	38.68	22.11	11	4.3	119
1983 Sep 11 10 49 58.9	38.73	22.39	18	4.0	79
1983 Sep 19 1 18 13.2	38.73	22.47	11	4.7	147
1983 Sep 19 1 29 56.8	38.75	22.40	20	4.3	92

PC: from the Papazachos & Comninakis (1986) catalogue.

UNS: from the UNESCO catalogue (Shebalin *et al.* 1974).

Note: These parameters are extracted from the Makropoulos *et al.* (1989) catalogue and Appendix. The first four entries are from the Appendix, which includes earthquakes with inadequate information to re-assess all parameters. The remaining earthquakes are extracted from the main catalogue, for which there is sufficient information to relocate and re-examine the parameters in the manner adopted by Makropoulos & Burton (1981).

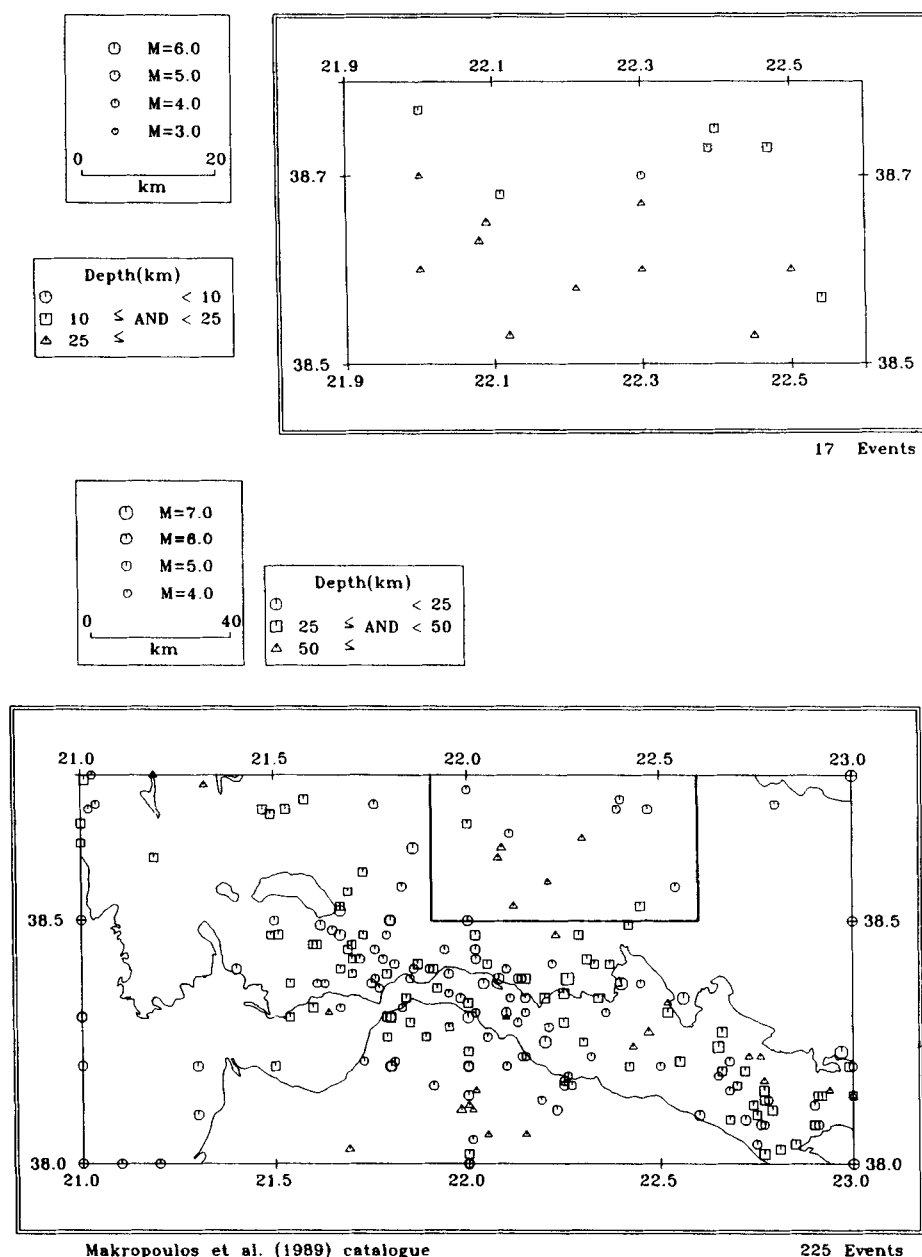


Figure 2. Distribution of large earthquakes in central Greece during 1900–1985, and an extracted window focusing on the Pavliani area (extracted from Makropoulos *et al.* 1989). The main diagram contains the earthquakes given in the main catalogue, and the window illustrates events from both the main catalogue and the accompanying Appendix. Surface-wave magnitudes, M_s , are plotted.

that several earthquakes, based on PATNET recordings only, relocate from close to the Patras area to the Pavliani area when the combined PATNET–VOLNET data set is used. This effect is due in particular to the small number of PATNET recordings available for these specific events and the location of Pavliani, which is approximately 100 km outside the Patras network. It was therefore decided to use only records from the Volos network, which includes the station at Pavliani, when studying crustal deformation in the Pavliani area.

2.2.1 Spatial distribution

The seismicity located in central Greece during 1983–84 (Fig. 4) shows a concentration of high seismicity in the Pavliani

area, with 402 recorded events of local magnitude between 1.3 and 4.6 M_L (Fig. 5a). A subset of 70 well-located events was chosen for detailed analysis (Table 3), selected using the following criteria:

- (1) 5 km maximum error in computed locations of both epicentre and depth;
- (2) a minimum number of five stations reporting clear P -wave recordings; and
- (3) a maximum computed root-mean-square traveltimes residual of 0.5 s.

A least-squares line fitted to the epicentres, illustrated in Fig. 5(a), shows a WSW–ENE trend. A similar trend is seen after applying the same procedure to the 70 well-located events

Table 2. Station details of Patras and Volos microearthquake networks.

Station Code	Station Site	Component (*)	Latitude (° min N)	Longitude (° min E)	Height (m)	Geological Foundation
PATNET						
PT1	University of Patras	Z N-S E-W	38 17.35	21 47.32	70	Pliocene conglomerate
PT2a	Tsoukaleika	Z	38 9.17	21 38.73	45	Pliocene conglomerate
PT2b	Kaminia	Z	38 8.58	21 36.80	25	Quaternary marine dep.
PT3a	Lakkopetra	Z	38 10.59	21 27.99	85	Eocene flysch
PT3b	Araxos	Z	38 11.29	21 22.95	45	Cretaceous limestone
PT4	Agia Trias	Z	38 23.43	21 19.91	5	Pliocene lagoonal dep.
PT5	Kato Vasiliki	Z	38 21.72	21 37.21	50	Eocene flysch
PT6	Molykreion	Z	38 21.18	21 44.84	55	Pliocene lacustrine dep.
VOLNET						
VSI	Simia	Z N-S E-W	38 52.76	23 12.54	448	Up. Pliocene sandy marl
VPA	Pavliani	Z	38 46.89	22 20.40	1084	Tertiary flysch
VFI	Filaki	Z	39 14.11	22 35.52	360	Cretaceous limestone
VGL	Glafira	Z	39 26.74	22 53.05	424	Trias.-Jurassic marbles
VNE	Neochorion	Z	39 18.71	23 13.93	692	Limestone
VSK	Skopelos	Z	39 6.64	23 41.61	374	Cretaceous limestone
VMA	Markates	Z	38 42.35	23 35.26	468	Jur.-Cretaceous schist
VTH	Erithrai	Z	38 12.03	23 21.60	756	Up. Triassic limestone
VAG	Agia Anna	Z	38 18.96	22 54.02	760	Up. Jurassic limestone

*: Willmore MkIII seismometers.

Z: vertical component; N-S and E-W: horizontal components.

(Fig. 5b). Thus, the Pavliani microseismicity defines a fault zone with a WSW–ENE trend. Its eastern extent coincides with a fault zone of the same trend mapped south of the village of Kaloscopi. Two cross-sections, along and perpendicular to the trend line, show a concentrated zone of seismicity. This zone is approximately vertical and extends from about 7 to 20 km depth (Fig. 6). Hence, a seismically active volume approximately 20 km long, 5 km wide and 13 km deep is defined by the 70 well-located events.

Two of the three 1983 earthquakes in the region that are documented in the Makropoulos *et al.* (1989) catalogue (Table 1) were also located by the Volos network. The event of 1983 September 11 was not located and is not included in the published Volos network bulletins. The local magnitude given by VOLNET is 4.6 M_L , in contrast with the surface-wave magnitude of 4.7 M_s in the Makropoulos *et al.* (1989) catalogue for the first event on 1983 September 19. The second earthquake on September 19 shows a similar difference: 4.2 M_L from VOLNET and 4.3 M_s from the Makropoulos *et al.* catalogue. The magnitudes given by VOLNET for these particular events were estimated using the amplitude of the first

P peak at each station, instead of the maximum S amplitude, which was used normally [being the usual Richter (1958) procedure], because the seismometers overloaded when the events were too big for the microearthquake-tuned Volos network. The epicentre locations given by Makropoulos *et al.* (1989) and the epicentres computed from the Volos network data for the two events agree to within 5 km. However, focal depths given for the two events are 8.3 km and 8.2 km, in contrast to 11 km and 20 km for the Volos network and Makropoulos *et al.* (1989) locations respectively.

2.2.2 Temporal variations

The distribution of local magnitude for the 402 events (Fig. 7a) shows that the seismicity in Pavliani consisted of two main swarms. The first occurred in 1983 April and the second in 1983 September. The magnitudes of these events are in the range 1.3 to 4.6 M_L , corrected to National Observatory of Athens standard local magnitudes. Fig. 7(b) shows the focal depth distribution as a function of time and demonstrates that little event migration took place in the zone of seismicity

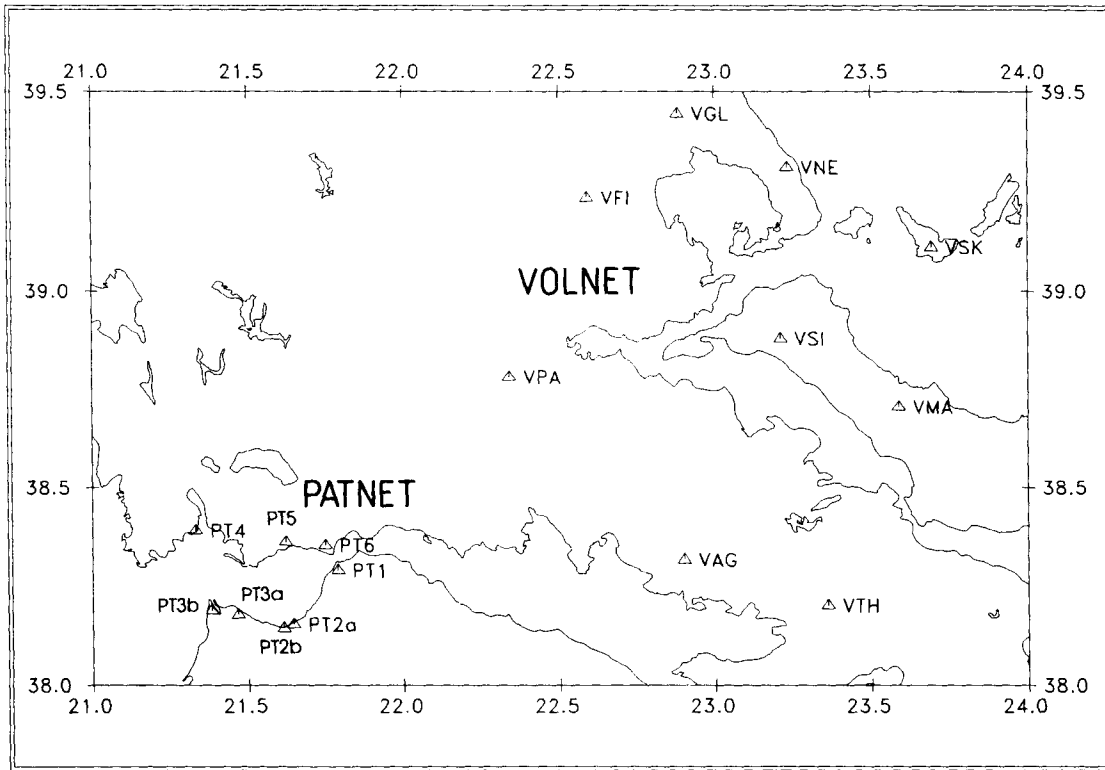


Figure 3. Volos Seismic Network (VOLNET) and Patras Seismic Network (PATNET) station locations.

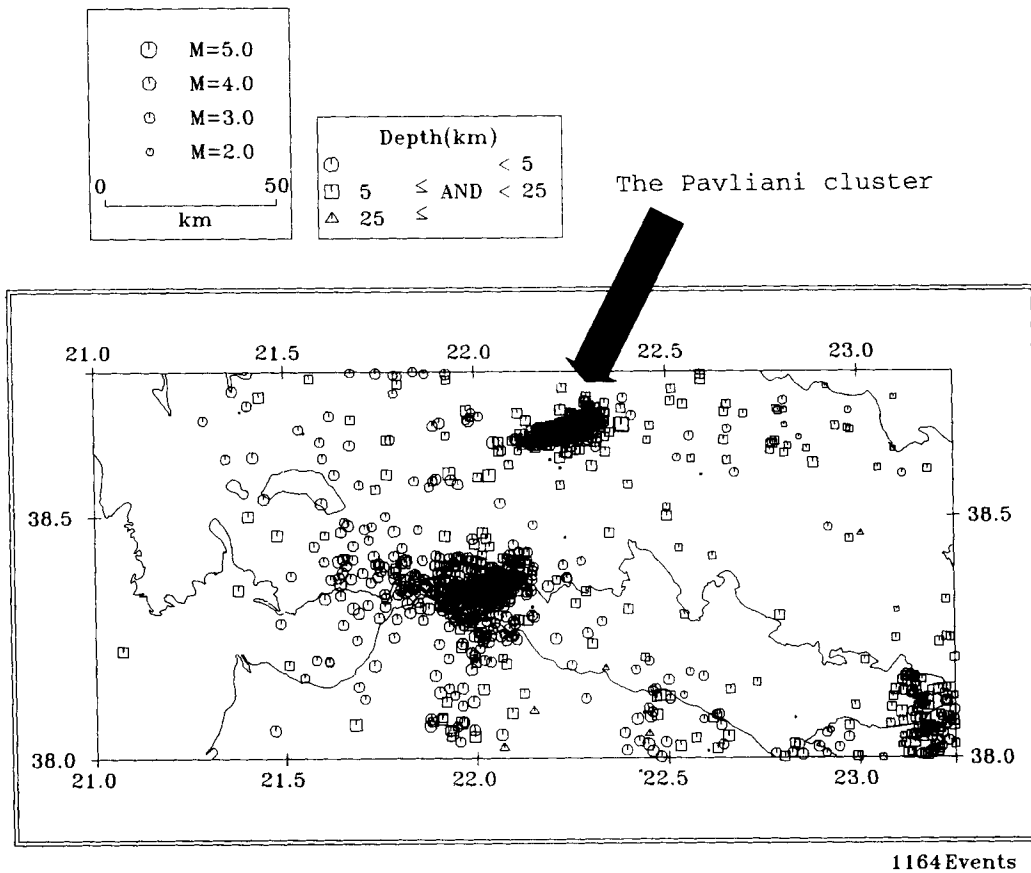


Figure 4. Epicentres in central Greece during 1983–84. The arrow shows the cluster of events in the Pavliani area. Local magnitudes, M_L , are plotted.

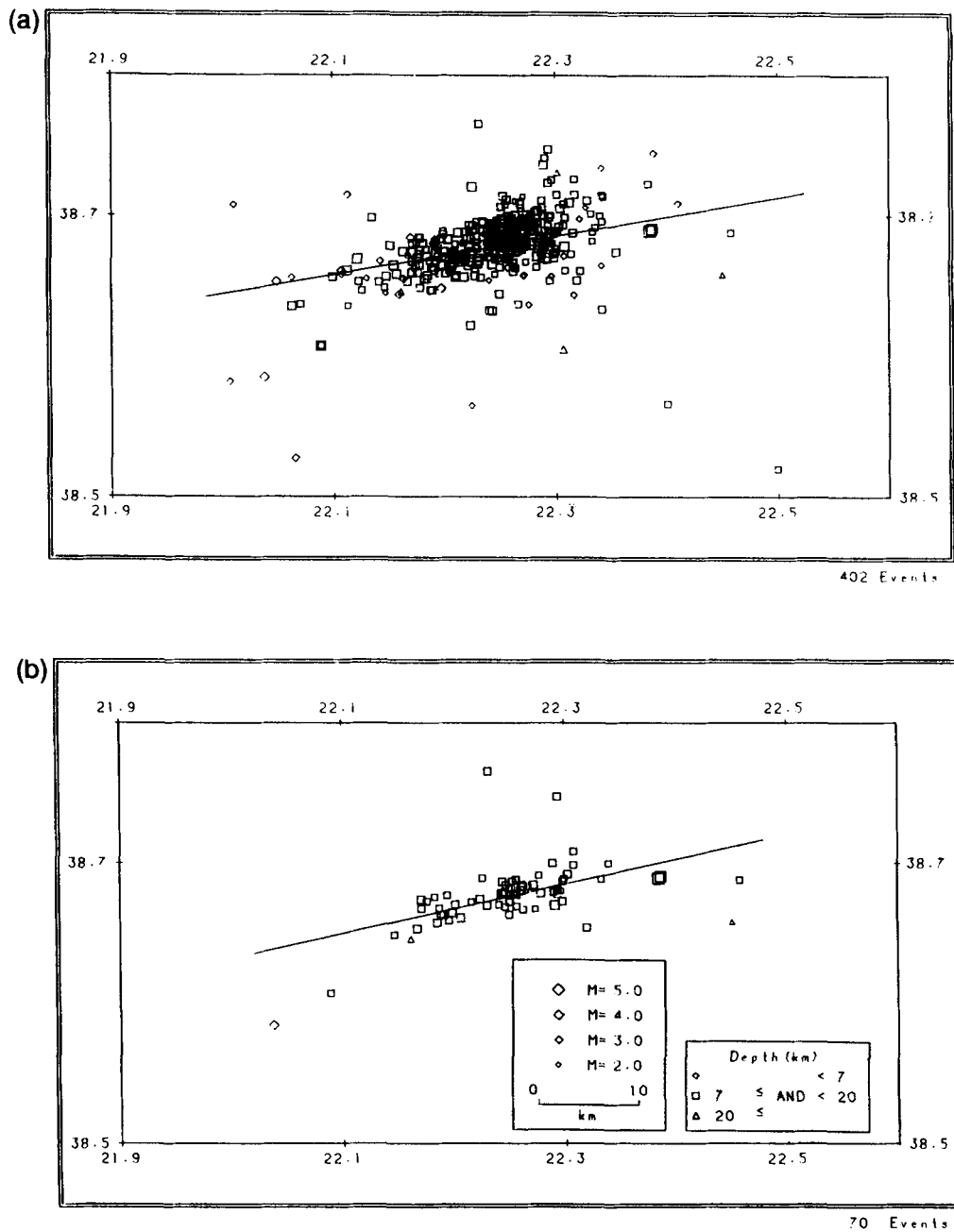


Figure 5. Seismicity located in the Pavliani area during 1983–84 (with line fitted in the least-squares sense to the epicentres). (a) All 402 recorded events and (b) the 70 well-located events (Table 3; see text for criteria). Local magnitudes, M_L , are plotted.

between the two swarms. However, it is apparent from Figs 5 and 6 that events with small magnitude, between 1.3 and $3.7 M_L$, occurred in the western and the central parts of the zone, whereas, by contrast, the eastern part includes two events with magnitude greater than $4 M_L$. The whole fault zone is active, with a large number of small-magnitude events in its western and central parts, and a smaller number of small-magnitude events plus some larger events in the eastern part.

2.2.3 Focal mechanism of the 1983 September 19 earthquake

In general, focal mechanisms could not be defined for the events located in Pavliani, because the observing station density

was usually insufficient. However, a fault-plane solution could be estimated for the largest earthquake, that of 1983 September 19 with magnitude $4.6 M_L$. For this earthquake, the Volos and Patras seismic networks first-motion data were used in conjunction with data provided by the National Observatory of Athens (1983) recorded on the National Greek Network. The focal mechanism indicates a normal fault with a WSW–ENE strike. This strike is similar to the trend line of seismicity mapped in the Pavliani area shown in Fig. 5. The fault-plane solution is thus consistent with an extensional regime dominating the neotectonics in the Pavliani area and is consistent with the results from seismotectonic studies in adjacent areas (see Fig. 8). Furthermore, the stations of the Volos seismic network

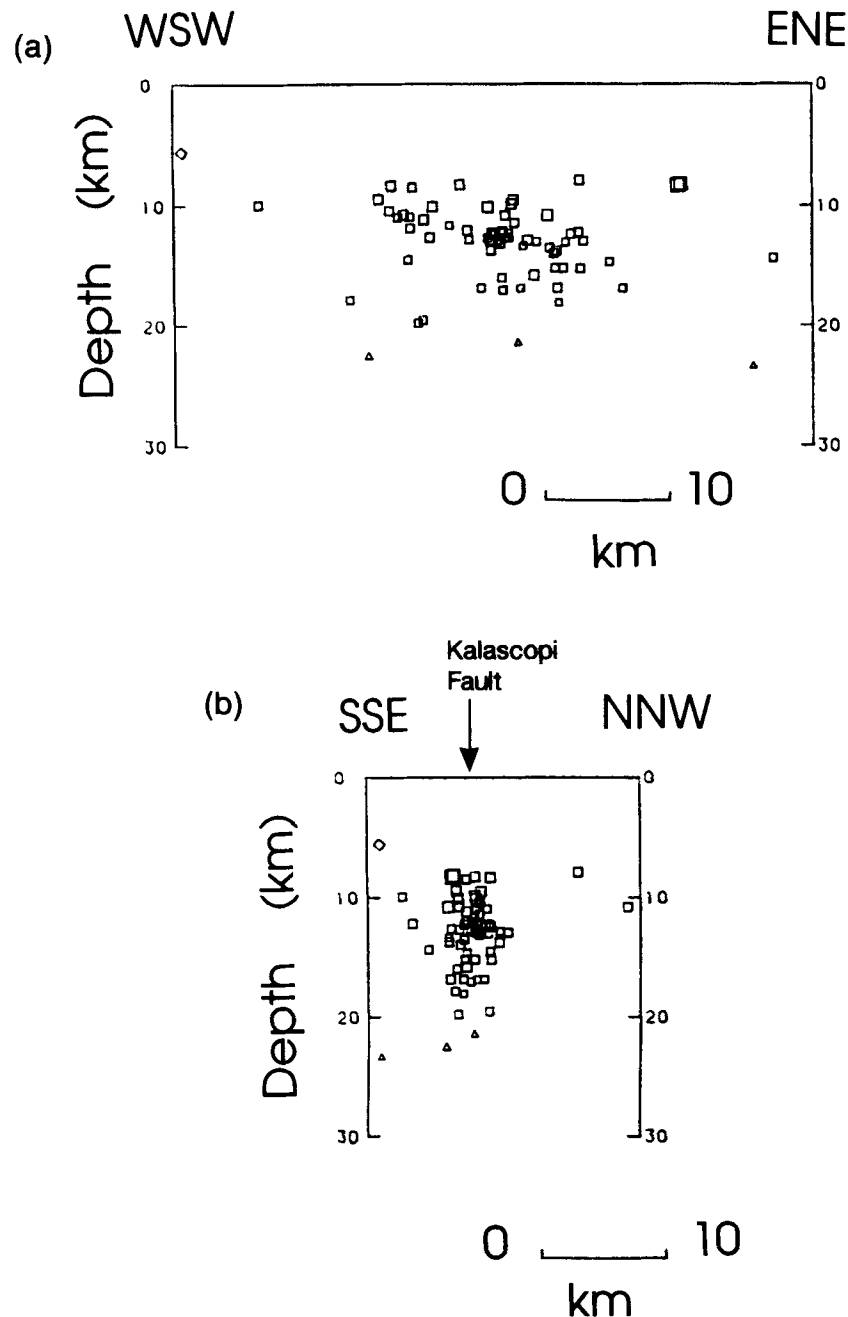


Figure 6. Cross-sections through hypocentres: (a) along and (b) perpendicular to the epicentral trend line illustrated in Fig. 5(b).

are seen to be well distributed amongst the three dominant quadrants in Fig. 8, and this is consistent with the averaging process on station spectral amplitudes to be carried out later.

3 SPECTRAL ANALYSIS OF MICROEARTHQUAKES AND COSEISMIC CRUSTAL DEFORMATION IN THE PAVLIANI AREA

The microearthquakes described above constrain a well-defined zone of seismicity within which coseismic deformation is taking place both through individual microearthquakes and through the cumulative effect of many microearthquakes. To examine the coseismic deformation in more detail, its relative

variation throughout the zone and its cumulative properties, we examine seismotectonic source parameters obtained through spectral analysis of the microearthquakes. There are many examples of the extraction of such parameters from spectra, including the studies of Keilis-Borok (1959), Trifunac (1972), Hanks & Wyss (1972), Thatcher & Hanks (1973), Archuleta *et al.* (1982), Modiano & Hatzfeld (1982), Gagnepain-Beyneix (1985), Brune *et al.* (1986) and Burton & Marrow (1989). All of these studies involve spectral analysis of *P*-wave data or *S*-wave data or both. In the present study, *P*-wave spectral analysis is applied to the 70 well-located events. The earthquake source parameters derived are seismic moment (M_0), stress drop ($\Delta\sigma$), source or 'fault' radius (r) and average coseismic slip (s).

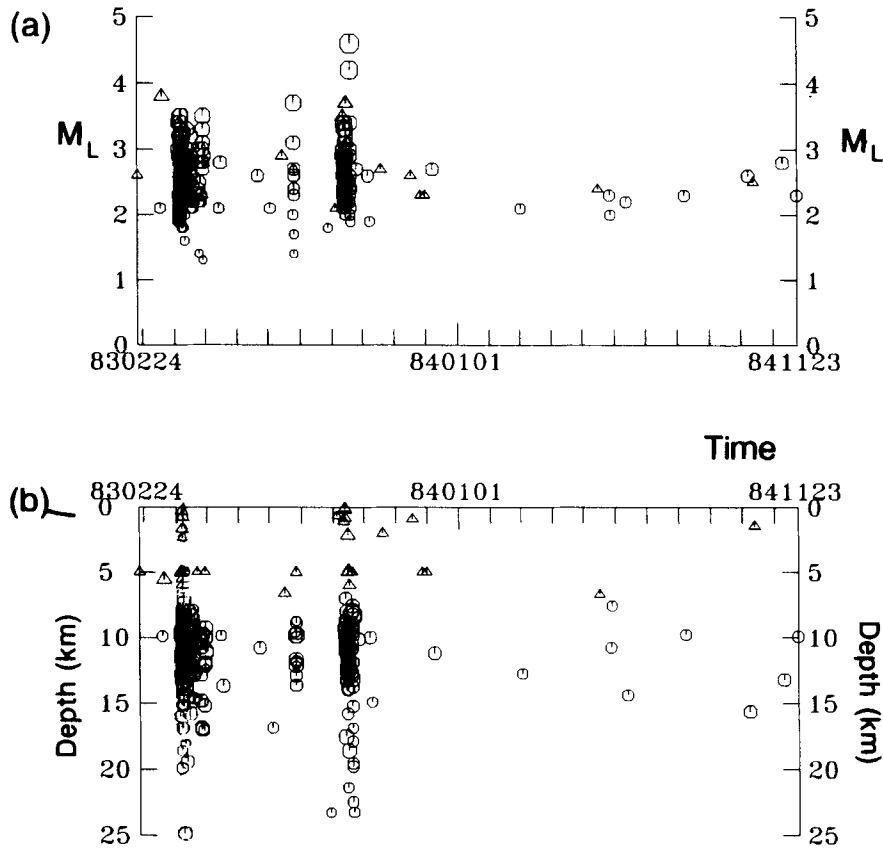


Figure 7. Temporal variation of microearthquake swarm activity in Pavliani (whole data set), (a) magnitude (b) focal depths. Time is expressed as: year-month-day.

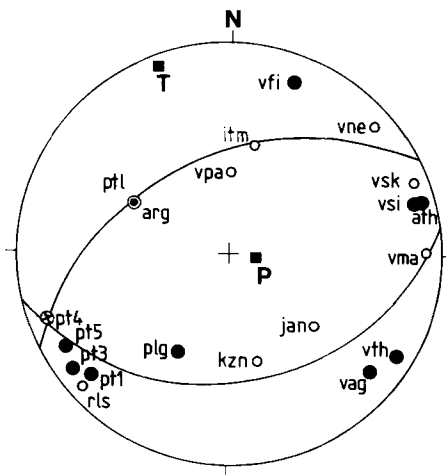


Figure 8. Focal mechanism solution for the earthquake of 1983 September 19, with local magnitude 4.6 M_L , plotted using an upper hemisphere equal-area projection. Compressions noted with black filled circles, dilatations with open circles, axes of compression and tension noted with black filled boxes. Station pt4 is noted with a crossed circle. It recorded an emergent P, thus it lies on one of the two nodal planes. Stations pt1 and arg plot on the same spot. The one recorded compression and the other dilatation, hence they are on either side of the nodal plane. The readings of stations vs1, ath, plg and rls are less reliable. The focal mechanism solution is:

	strike	dip	plunge	plunge dir.
Plane 1:	242	52	P-axis: 79	271
Plane 2:	258	40	T-axis: 05	158

3.1 Methodology adopted and problems involved

The procedure involves a standard Fourier spectral analysis of a selected time window in the seismogram (in our case the *P*-wave window). A 'typical' *P*-wave displacement spectrum is characterized by a flat section with amplitude level Ω_0 up to a frequency f_c , and a roll-off linear decay from f_c to an f_{max} . The long-period spectral level and the corner frequency are defined by two intersecting lines that are fitted by eye to the overall mean trend of the low-frequency spectral asymptote and the high-frequency roll-off or decay. These are the parameters used to determine the source characteristics of each analysed event. In practice, the two most important considerations are those of window selection and attenuation.

An existing spectral analysis package (Evans, McGonigle & Fyfe 1985) was revised. In the final package, standard Fourier spectral analysis and time series preparation of a selected digital seismogram window of 2^N samples length for integer N , instrument correction, cosine tapering, noise removal and smoothing (based on Burton & Blamey 1972) are performed to output the required displacement spectrum. A *Q*-correction for frequency-independent *Q* fixed along the propagation path is also included, and, thus, two separate spectra, with and without the *Q*-correction respectively, are produced (Melis 1992). A typical example of the output for further analysis consists of three graphs:

- (1) the original seismogram with defined noise and signal windows;
- (2) the displacement spectrum corrected for instrument response; and

Table 3. Hypocentral coordinates, magnitudes and location errors for the 70 well-located events recorded by VOLNET near Pavliani. Magnitudes have been calculated in the normal way (Richter 1958). Otherwise where P is indicated, only first P amplitudes have been used because the recording system was overloaded. Where N is indicated, only vertical components were used. In addition, for the present study a correction (+0.3) was suggested (Burton *et al.* 1991) and was applied in order to convert these M_{LV} magnitudes to standard M_L local magnitudes.

Event No	Origin time (Y-M-D hr min sec)	Latitude (°N min)	Longitude (°E min)	Depth (km)	M_L	RMS (sec)	ERR (km)	ERZ (km)
1	83 320 8 25 56.17	38 35.08	22 2.27	5.57	3.8P	0.24	2.7	1.1
2	83 4 4 13 30 24.39	38 40.93	22 15.01	12.96	2.0	0.34	3.1	2.7
3	83 4 4 21 17 46.62	38 40.15	22 15.41	16.01	2.3	0.49	4.2	3.0
4	83 4 4 22 17 54.45	38 40.03	22 16.41	13.37	1.9	0.43	3.5	2.7
5	83 4 6 9 51 40.87	38 40.36	22 17.89	16.87	2.6	0.41	2.6	1.6
6	83 4 6 12 37 34.70	38 39.24	22 19.17	12.20	2.6	0.21	2.8	4.4
7	83 4 6 15 57 54.46	38 40.67	22 15.27	12.10	2.5	0.48	3.4	3.5
8	83 4 6 16 34 15.42	38 40.05	22 10.28	10.41	2.6	0.50	3.4	1.9
9	83 4 6 21 11 25.43	38 40.75	22 14.77	12.20	2.3	0.47	3.8	2.6
10	83 4 6 21 29 7.75	38 40.34	22 15.03	12.25	2.4	0.45	3.5	3.4
11	83 4 6 22 17 25.45	38 39.79	22 11.44	8.49	2.4	0.47	4.0	3.2
12	83 4 7 5 52 58.98	38 44.85	22 17.61	7.89	2.7	0.18	2.1	2.3
13	83 4 7 7 42 34.61	38 40.36	22 10.58	10.95	2.2	0.47	3.4	2.2
14	83 4 7 7 53 16.76	38 40.01	22 15.76	12.63	2.3	0.33	2.8	2.6
15	83 4 7 9 24 42.05	38 40.64	22 15.42	12.67	2.3	0.42	3.8	3.4
16	83 4 7 14 17 27.69	38 40.22	22 14.46	16.88	2.2	0.45	4.6	2.4
17	83 4 7 15 57 54.12	38 41.32	22 15.38	12.28	2.2	0.45	3.7	2.8
18	83 4 7 17 1 44.59	38 39.45	22 11.11	10.74	2.9	0.46	4.2	3.1
19	83 4 7 17 6 34.14	38 41.23	22 17.91	15.20	2.4	0.36	2.8	2.0
20	83 4 7 17 32 15.50	38 40.83	22 17.64	15.19	2.3	0.28	2.2	1.4
21	83 4 7 22 8 24.92	38 40.46	22 13.43	8.26	2.8N	0.21	1.8	4.3
22	83 4 8 2 57 46.47	38 41.06	22 16.31	12.90	3.0N	0.35	2.7	2.1
23	83 4 8 3 50 53.17	38 41.21	22 14.64	12.44	2.6	0.39	3.2	2.0
24	83 4 8 9 43 18.06	38 40.76	22 17.41	13.51	2.3	0.33	2.8	2.5
25	83 4 8 14 50 32.42	38 40.55	22 11.00	14.52	2.2	0.45	4.8	4.5
26	83 4 8 14 58 41.12	38 40.83	22 15.65	9.84	3.0	0.37	2.4	2.8
27	83 4 8 17 12 31.07	38 40.34	22 12.97	11.66	2.0	0.45	3.7	2.3
28	83 4 8 23 29 36.07	38 41.00	22 15.75	11.41	2.5	0.39	3.5	3.3
29	83 4 9 0 27 6.62	38 40.44	22 10.26	8.33	2.9	0.48	3.5	2.4
30	83 4 9 0 29 19.58	38 40.81	22 17.81	18.08	1.8	0.44	3.5	2.4
31	83 4 9 2 21 41.57	38 41.24	22 15.17	12.23	2.3	0.44	3.6	2.7
32	83 4 9 2 26 22.80	38 41.08	22 14.82	12.30	2.3	0.49	3.3	2.4
33	83 411 17 51 14.73	38 39.80	22 15.01	13.72	2.5	0.12	1.1	0.8
34	83 411 21 19 45.56	38 40.69	22 14.71	12.87	2.6	0.38	3.4	1.9
35	83 412 17 41 50.36	38 40.91	22 15.14	13.17	2.2	0.49	4.0	2.4
36	83 412 20 47 16.00	38 40.08	22 11.23	10.93	2.2	0.34	3.2	2.0
37	83 413 21 3 38.79	38 40.69	22 14.62	10.11	3.3N	0.39	2.5	1.7
38	83 414 12 13 58.57	38 40.72	22 16.71	15.81	3.0	0.42	2.8	1.8
39	83 417 15 21 33.41	38 39.78	22 11.33	11.88	2.5	0.36	5.0	2.1
40	83 417 17 6 34.86	38 40.23	22 12.10	12.68	2.7	0.37	3.0	1.7
41	83 418 0 36 30.77	38 41.32	22 19.99	14.65	2.1	0.38	4.1	2.2
42	83 427 10 17 46.72	38 40.64	22 15.32	17.07	2.2	0.26	2.2	1.5
43	83 429 1 1 44.01	38 39.66	22 12.39	10.09	3.0N	0.39	2.9	2.1
44	83 429 5 1 6.60	38 40.19	22 13.83	12.05	2.7	0.47	3.8	2.0
45	83 430 3 40 36.81	38 39.87	22 11.93	11.18	2.9	0.46	3.4	1.9
46	83 621 18 36 8.69	38 45.94	22 13.88	10.79	2.6	0.41	2.8	1.9
47	83 7 3 7 26 1.43	38 42.00	22 20.39	16.86	2.1	0.42	3.0	2.2
48	83 828 21 59 25.11	38 39.49	22 27.04	23.27	1.8	0.10	3.7	3.1
49	83 913 16 2 18.77	38 41.36	22 13.57	12.83	2.2	0.27	4.2	2.8
50	83 914 12 2 14.35	38 40.20	22 17.47	10.79	3.4N	0.32	4.8	3.1
51	83 914 12 33 26.27	38 39.19	22 10.03	9.44	2.9N	0.50	4.6	5.0
52	83 914 13 56 49.47	38 40.67	22 17.62	13.96	2.5	0.30	2.7	2.4
53	83 914 16 18 59.07	38 41.48	22 16.61	13.02	2.1	0.46	3.5	3.3
54	83 914 18 27 26.19	38 40.85	22 15.93	21.36	2.0	0.32	3.8	1.5
55	83 914 18 32 56.06	38 41.34	22 17.97	13.03	2.1	0.26	2.9	4.6
56	83 914 21 35 44.27	38 41.52	22 18.17	12.34	2.7	0.44	3.4	3.3
57	83 919 1 18 13.03	38 41.35	22 23.09	8.29	4.6P	0.21	2.6	2.5
58	83 919 1 29 56.39	38 41.43	22 23.21	8.20	4.2P	0.23	2.7	2.6
59	83 919 1 39 45.53	38 40.63	22 11.66	19.54	2.3N	0.14	3.6	4.4
60	83 919 1 43 33.77	38 40.13	22 14.78	12.68	2.3	0.48	4.6	4.1
61	83 919 2 25 3.93	38 41.06	22 15.67	9.51	3.0	0.50	3.9	4.0
62	83 919 2 35 7.08	38 38.75	22 9.69	22.46	2.2	0.18	4.3	1.3
63	83 919 3 27 46.69	38 38.92	22 8.80	17.88	2.2	0.05	1.0	0.5
64	83 919 3 46 25.30	38 39.54	22 11.75	19.79	2.3	0.13	2.6	1.3
65	83 919 5 21 16.90	38 42.50	22 18.46	12.93	2.4	0.34	2.8	4.3
66	83 919 15 56 21.72	38 42.00	22 17.36	13.76	2.6	0.34	2.6	1.8
67	83 919 18 57 15.43	38 41.92	22 18.49	15.23	2.4	0.26	2.0	1.4
68	83 919 22 29 7.99	38 40.98	22 16.03	16.88	2.0	0.25	2.7	4.5
69	84 612 23 0 0.69	38 41.28	22 27.46	14.38	2.2	0.31	3.3	4.7
70	841123 20 7 41.05	38 36.43	22 5.35	9.93	2.3	0.32	3.0	3.2

(3) an equivalent to (2) corrected also for Q along the propagation path.

Noise correction can be applied in cases (2) and (3), whereupon the noise-equivalent spectra are also produced. However, acceptable observations in the first instance do have clear P -wave recordings as one of the criteria for well-located events described in Section 2. There is a further facility (Abercrombie 1991) allowing examination of the time-domain displacement seismogram in addition to the displacement spectrum. The combination of clear P waves, inspection of displacement seismograms, and generation of noise corrected spectra as necessary, is consistent with preparing station spectra from which Ω_0 may be measured and averaged.

To produce these graphs in practice, Fourier analysis is performed on two equal-length windows sampling noise and signal respectively. Both seismogram windows are cosine-tapered by 5 per cent on both back and front ends in the time domain. This is done in order to eliminate any truncation effects and to reduce the high-frequency lobes which are introduced by the use of a simple box window (Burton & Marrow 1989). Willmore MkIII velocity transducers are used in the network, and so a conversion from velocity to ground displacement and a correction for the instrument response are made in the frequency domain prior to output of the spectrum. The record-replay system used had a flat response to ground velocity from 0.67 to 16 Hz. Hence f_c was acceptably defined and measured only when its value was strictly less than 16 Hz. In addition, the noise correction can be made if required by simple subtraction of noise from signal Fourier amplitudes in the frequency domain. The final step is the correction for a fixed Q along the propagation path. The more significant problems of this analysis and the adopted solutions applied to the 70 well-recorded events now follow.

3.1.1 Windowing and Q -correction

Extensive trials were made in an attempt to determine a satisfactory convention that systematically defines the window prior to spectral analysis, and to determine when a Q -correction is appropriate. The aim is to define a window that envelopes the P phase and P coda, undisturbed if possible by other crustal phases. Secondly, the effect of the Q -correction on both the low-frequency spectral level and corner frequency was investigated for three hypocentral distance ranges.

It has been noted in some previous studies that, for small magnitude events, Q -correction is not necessary for epicentral distances of less than 50 km (Street, Herrmann & Nuttli 1975). For short distances, very little or no information in terms of spatial Q can be retrieved from the signal coda. Brune *et al.* (1986) suggested that Q -correction is not essential as it does not change the spectral characteristics. Fletcher *et al.* (1986) showed that Q -correction does not change the spectrum asymptote or the decay dramatically. Thus, Q has frequently been ignored, either because it was held to be large (negligible attenuation) or because there was insufficient information to define it usefully. However, Anderson (1986) argued that a Q -correction is necessary as the true spectral decay is affected by a frequency-dependent Q , ($Q(f)$), which rolls off at high frequencies in a similar way to the true spectral decay. Archuleta *et al.* (1982), Gagnepain-Beyneix (1985), Brune *et al.*

(1986), Fletcher *et al.* (1986) showed that whether Q is frequency-dependent or constant does not affect significantly the Ω_0 and f_c observed on a log-log spectrum.

A further potential problem is the influence of significant weathered layers. Up- and down-borehole observations in some cases suggest P -wave Q in the range 6.5 to 27 in the upper 300 m (Aster & Shearer 1991) and high-frequency (about 2 Hz) Rayleigh waves in some cases suggest S -wave Q in the range 11 to 50 in the top 400 m (MacBeth & Burton 1987), causing substantial loss of high-frequency signal content, which is uncorrectable when lacking detailed *in situ* observations. Abercrombie & Leary (1993) drew attention to similar difficulties in comparing up- and down-hole spectra in a situation in which the up-hole seismometer was sited on a rock column known to consist of 500 m of sediments followed by 200 to 300 m of highly fractured granite. These last concerns are largely eliminated in the Volos network by seismometer placements carefully sited on bedrock, usually limestone (Table 2).

In this study, Q was assumed constant along the propagation path. The method tested by Archuleta *et al.* (1982), and others, was used employing an exponential function to describe the effects of absorption in terms of frequency (f), phase velocity (v) and propagation distance (R):

$$D(f) = \exp(-\pi f R / v Q) \quad (1)$$

The adopted value of Q^{-1} is 0.003, which is consistent with Delibasis (1982), Condon (1985) and Hashida *et al.* (1988) for the Aegean region.

Few previous studies have made a systematic attempt to consider the effects of varying window length on the spectra. Modiano & Hatzfeld (1982) tried window lengths varying from 0.25 to 3.50 s for P waves and noticed no significant changes in the spectral characteristics; they opted to use a window length of 1.0 to 1.5 s. Gagnepain-Beyneix (1985) tested P -wave window lengths of 1 and 2 s, and concluded that a factor of 2 was the maximum resultant change in the low-frequency level, with no change in the corner frequency. Thus, he fixed the P -wave window length to the minimum $t_s - t_p$ time (time window between P and S arrivals) expected in the whole data set for analysis. Burton & Marrow (1989) tested P -wave windows of 2 s, 5 s and 25 per cent of $t_s - t_p$. They concluded that the long-period spectral level changed by a factor of 2 to 3, while the change in the corner frequency was not apparent by eye. Thus, they decided to use window lengths up to 25 per cent of $t_s - t_p$, but chosen by eye in order to exclude any other crustal phases appearing within the selected window lengths.

In the present study, it was necessary to ensure that the 5 per cent cosine tapering applied back and front to the selected window for spectral analysis did not disturb the beginning of the P phase. Thus, the window had to start prior to the P arrival. This allowance depends on the value of $t_s - t_p$, and for the Pavliani seismicity a length of 0.5 s prior to the observed P -wave arrival was found to be sufficient to cover all possibilities for the recording stations.

Windowing conventions and influence of the Q -correction have been investigated extensively for microearthquakes in Greece (Abercrombie 1991; Burton *et al.* 1991; Melis 1992), and in this study the microearthquakes were classified into three hypocentral distance categories (a close approximation to propagation distance) to see if measurements of Ω_0 and f_c

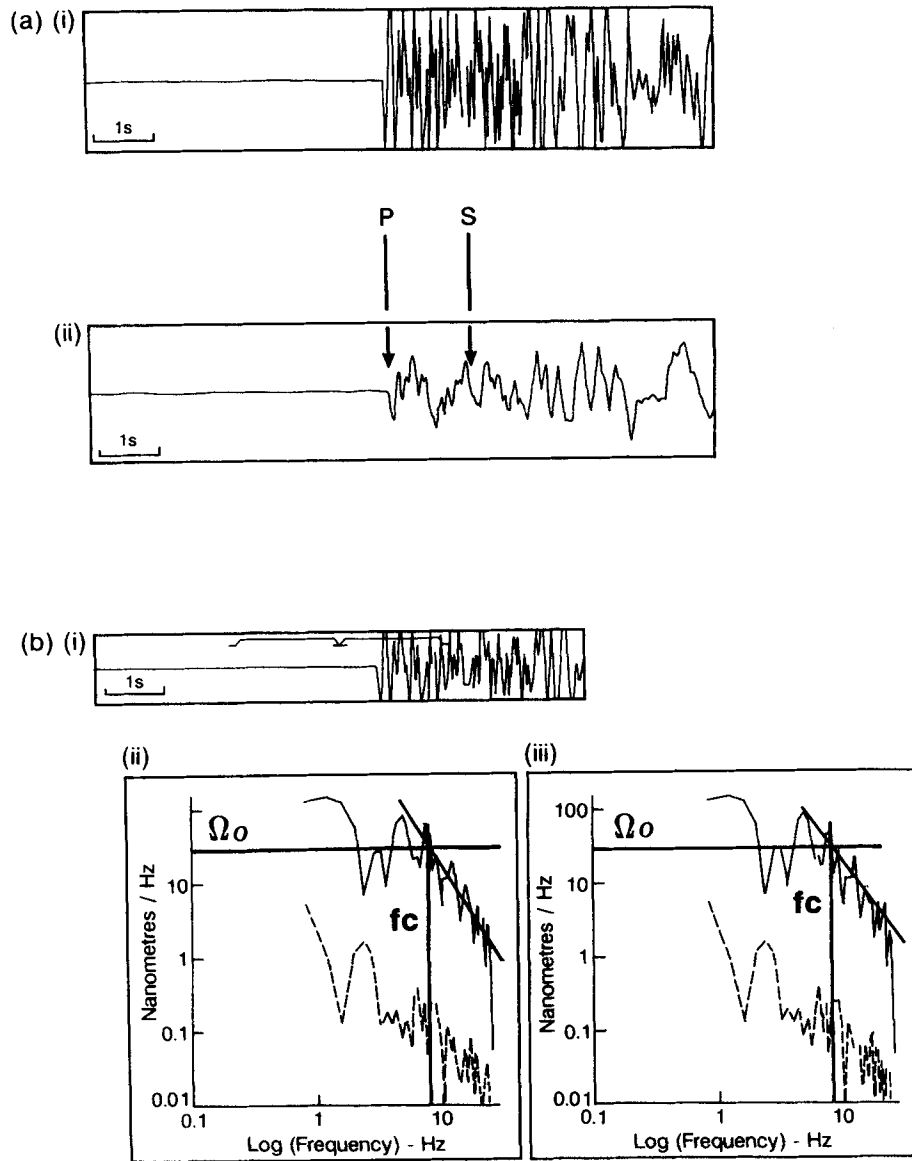


Figure 9. Spectral analysis for short hypocentral distances (< 10 km). (a) The original velocity seismogram is illustrated in (i) and the deconvolved displacement seismogram in (ii). (b) The selected window is illustrated in (i) and the instrument-corrected and Q -corrected spectra in (ii) and (iii), respectively. (The example is earthquake number 12, 1983 April 7, recorded at station VPA with hypocentral distance 9.6 km.)

were affected (Figs 9–11). A useful adjunct to the windowing procedure was the use of filtered displacement seismograms (Abercrombie 1991) produced by deconvolution of the original instrument-corrected spectrum. Displacement seismograms can be inspected next to the original velocity seismogram to assist with investigation of the P coda and allow the P arrival, P phase, P crustal phases, P_n phase, S arrival and S phase to be more easily identified.

For hypocentral distances less than 10 km, t_s-t_p is expected to be less than 2 s, and the Q -correction does not affect spectral measurements (Fig. 9). These very short hypocentral ranges apply to a small percentage of the data (≈ 5 per cent). For hypocentral distances in the range 10–40 km, clear crustal reflections may appear before the S arrival (Fig. 10). Tests using different lengths of the t_s-t_p interval resulted in only very small changes in the spectra. The Q -correction does not

significantly affect these measurements, although the P crustal phase apparent within the P coda is responsible for small increases in Ω_0 which were observed when using windows encompassing large percentages of the t_s-t_p time. The window finally selected ends prior to the arrival of the P crustal phase. Thus, although the effect of the P crustal phase commonly observed in the P coda is minor, it was nevertheless excluded from the windows finally selected. For hypocentral distances greater than 40 km, additional P crustal phases and P_n can appear (Fig. 11). This is important because, if the window includes more than one P phase (or S -to- P conversion), we are then looking at the equivalent to multiples of a P -energy source. Measurements on the instrument-corrected spectrum of the crustal phase (Fig. 11b) produced an Ω_0 and an f_c similar to those obtained from the first P -phase arrival (Fig. 11c). This is typical for one of the P crustal phases, and demonstrates a

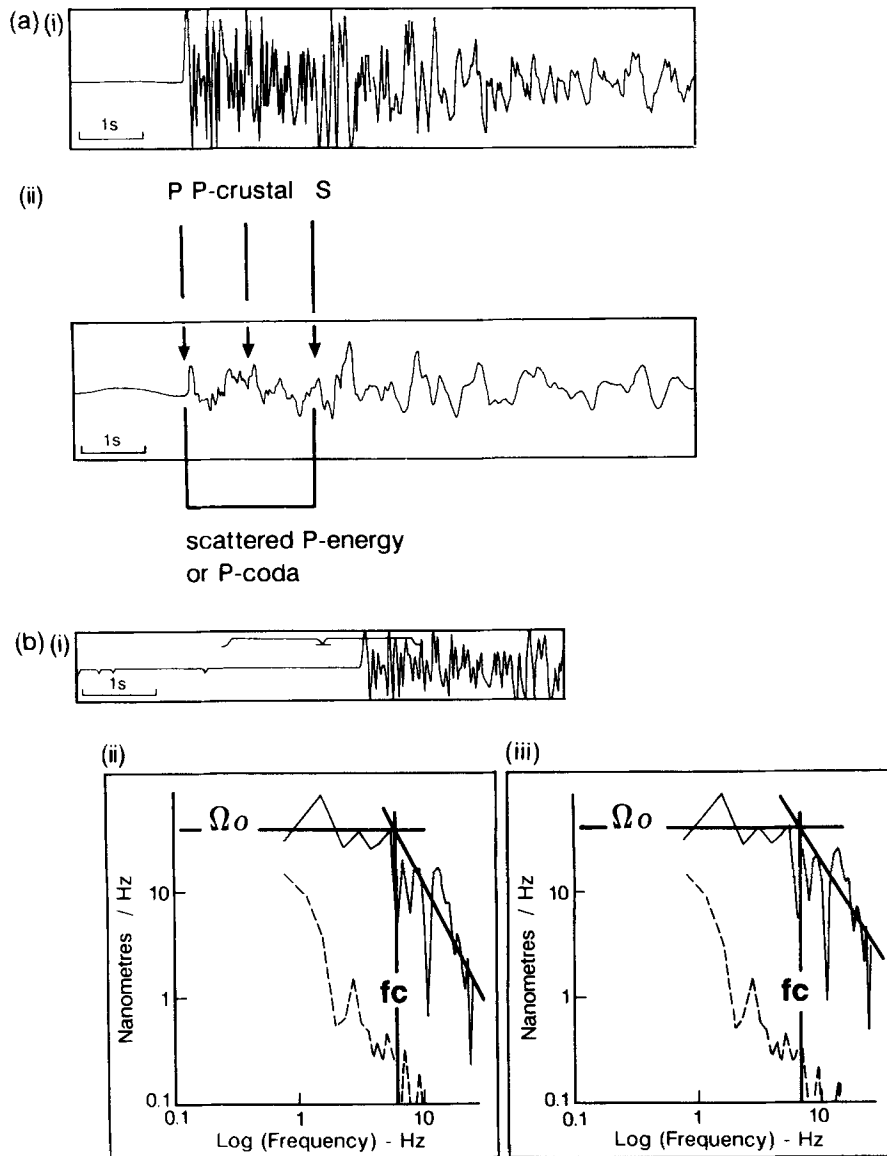


Figure 10. Spectral analysis for middle hypocentral distances (10–40 km). Figure format is as described in the caption to Fig. 9. (The example is event number 49, 1983 September 13, recorded at station VPA with hypocentral distance 19.2 km.)

multiple of the *P* energy included within the *P* coda (Fig. 11a). One reason for an apparently increasing Ω_0 and slight changes in f_c is the introduction of *P* crustal phases accompanying lengthening of the selected window. The high-frequency asymptote of *Q*-corrected spectra in this third distance category changes with increasing window length; however, changes in the measured Ω_0 and f_c are within 20 nm Hz^{-1} and 2 Hz, respectively, and significant changes in the parameters measured from the *Q*-corrected spectra are not introduced. The window finally selected encapsulates the first *P* phase (Fig. 11c) and ends prior to the arrival of the first *P* crustal phase. Very similar values were measured on an equivalent spectrum for the *P* crustal phase, demonstrating that the multiple of the *P* phase has nearly identical spectral properties. A combination of two phases, however, may give rise to slightly different estimates of source properties.

These three categories lead to the conclusion that windowing

should not be selected with a single convention if the source parameters are to be estimated optimally. Each seismogram record ought to be examined individually, and the criteria discerned above used for the correct window selection and analysis.

Hence, for all categories, the window starts 0.5 s prior to the *P* arrival and extends as far into the *P* coda as it can without encapsulating and being contaminated by other *P* crustal phases or *S*-to-*P* conversions etc. The window stops before the *S* arrival. *Q*-correction causes no visible spectral change in the first distance category, and only slight changes in the second at high frequencies. However, in neither case does this influence the measurement of Ω_0 or f_c . In the third distance category, *Q*-correction causes spectral changes, although there is little visible influence on the measurement of Ω_0 or f_c . However, *Q*-correction is applied because the high-frequency roll-off is significantly affected by *Q*.

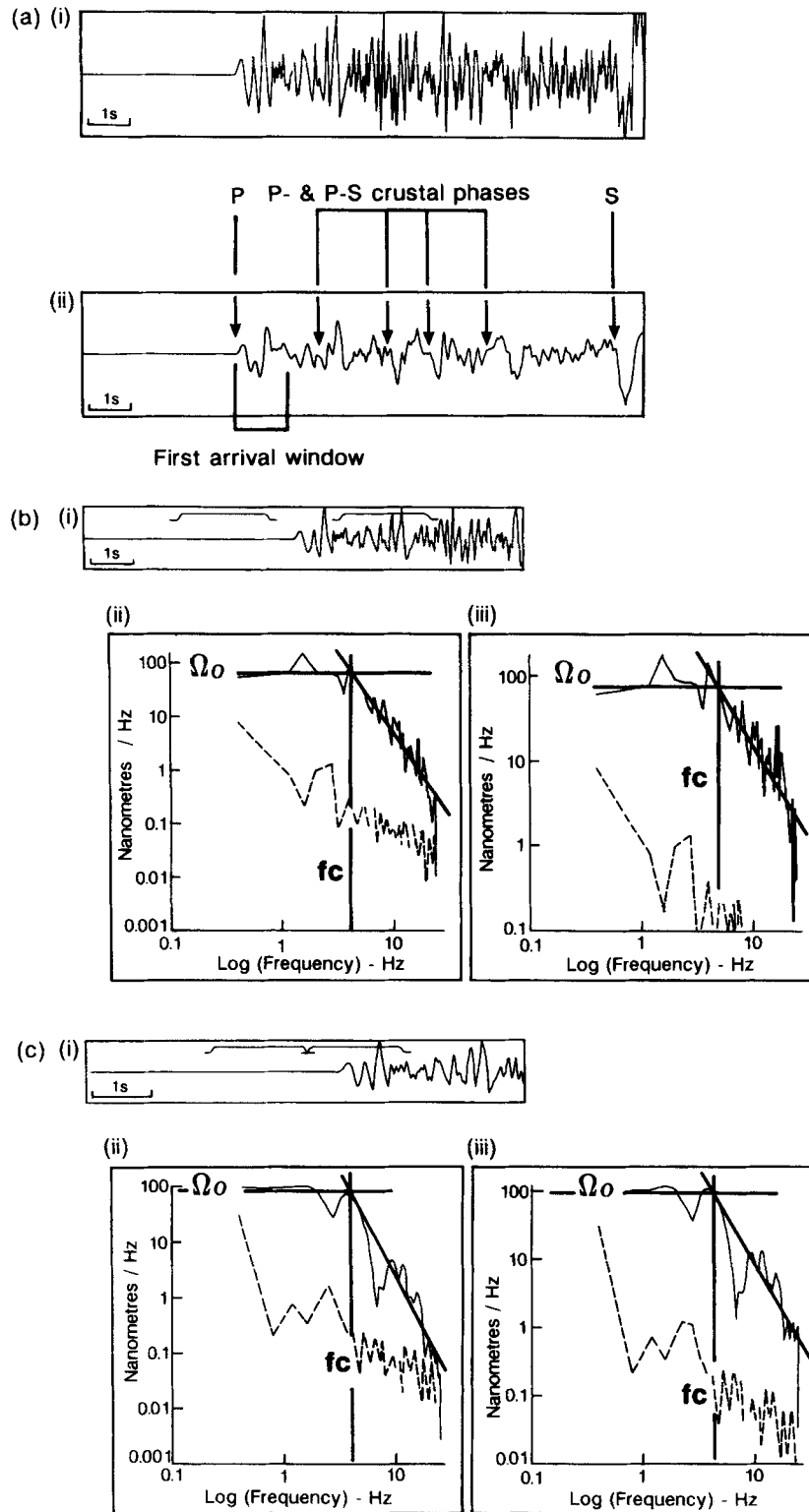


Figure 11. Spectral analysis for long hypocentral distances (>40 km). Note *P*, *P*-crustal or *P*-to-*S* converted and *S* phases in the deconvolved displacement seismogram. Figure format is as described in the caption to Fig. 9, except that (b) encapsulates one *P* crustal phase and (c) encapsulates the first *P* phase arriving at the recording station. (The example is earthquake number 50, 1983 September 14, recorded at station VAG with hypocentral distance 66.9 km.)

3.2 Seismotectonic parameters of microearthquakes in Pavliani

The spectral analysis procedure described above was applied to all 70 well-located events to obtain estimates of Ω_0 and f_c . More than 1000 spectra were examined. Following the model of Brune (1970, 1971), the low-frequency spectral level Ω_0 is assumed to be proportional to the seismic moment M_0 , and is given by the equation (after Keilis-Borok 1959)

$$M_0 = 4\pi R \rho \alpha^3 \Omega_0 / k R_{\theta\phi} \quad (\text{in N m}), \quad (2)$$

where ρ is the density of the medium (2700 kg m^{-3}), R is the hypocentral distance between source and receiver, α is the P velocity at the source taken from the velocity model used to locate the events (Burton *et al.* 1991), and the product $k R_{\theta\phi}$ is a constant (commonly taken as 0.85), with the components k and $R_{\theta\phi}$ representing free-surface reflection and the average radiation pattern, respectively. Modiano & Hatzfeld (1982) found Madariaga's dynamic model (1976) to be more realistic than Brune's, and it is used here for the calculation of source radius r . This is proportional to the corner frequency, f_c , for a circular model of fault rupture, and, for a rupture velocity of 0.9β ,

$$r = 0.32\beta/f_c \quad (\text{in m}) \quad (3)$$

(Madariaga 1976), where β is the S -wave velocity at the source (β is taken as $\alpha/1.78$ after King *et al.* 1985) and f_c is measured from a P -wave spectrum. Assuming the case of complete stress drop for a circular fault, the average stress drop ($\Delta\sigma$) is obtained from

$$\Delta\sigma = 7M_0/16r^3 \quad (\text{in bars}) \quad (4)$$

(Keilis-Borok 1959; Kanamori & Anderson 1975), where M_0 and r are the values obtained previously. Slip s , averaged over a circular fault area, is given by

$$s = M_0/\mu\pi r^2 \quad (\text{in m}) \quad (5)$$

(Brune 1968), where μ is the shear modulus (typically $3 \times 10^{10} \text{ N m}^{-2}$). Seismic moments and fault radii are determined by averaging the values calculated for each station. Measurements of both seismic moment and fault radius are log-normally distributed, and so the best estimates are the geometric means (Archuleta *et al.* 1982). Most, but not every, seismogram produces a spectrum from which Ω_0 and f_c can be measured, despite the criteria for well-recorded and well-located earthquakes, and hence the number of Ω_0 and f_c observations is sometimes less than the number of observing stations. The averaging process is appropriate in relation to focal mechanism for Ω_0 and the ensuing seismic moment, since the expected dominant focal mechanism (see Fig. 8) generates observations in the three dominant quadrants in which the Volos seismic stations are well-distributed. Implicit averaging of corner frequency values to obtain source radius implies fewer complications than does averaging of Ω_0 , simply because f_c will not be influenced by the radiation pattern unless the pattern is frequency-dependent. Rather than giving a standard deviation on the resulting estimates of the means of seismic moment and fault radii, maximum and minimum values are calculated to show the overall range within which these parameters lie. A similar procedure is followed to determine stress drop and average slip (Gagnepain-Beyneix 1985), again including minimum and maximum values as well as the best estimate of each parameter. All results are tabulated in Table 4.

Results were obtained from successful spectral analysis of 66 of the 70 well-located events in the Pavliani area. The main features of these results in Table 4 are:

- (1) seismic moment in the range 1 to $95 \times 10^{12} \text{ N m}$;
- (2) source radius in the range 65 to 226 m;
- (3) stress drop in the range 5 to 103 bars; and
- (4) average seismic slip in the range 2 to 32 mm.

The results demonstrate a wide range of stress drops (5 to 103 bars) for events with local magnitude 1 to 4.2 M_L and seismic moment 1 to $95 \times 10^{12} \text{ N m}$. Stress drop is observed to be directly related to average coseismic slip (Fig. 12a). Source radius is approximately constant or, more meaningfully, varies only slowly for a wide range of stress drops and average coseismic slips (Figs 12b–c). In the Pavliani fault zone it appears that faults of similar size produce low as well as high stress drop and average coseismic slip events.

3.3 Coseismic crustal deformation in the Pavliani fault zone

To investigate coseismic crustal deformation, not of single microearthquakes, but of the total seismicity represented by the whole microearthquake data set, it is necessary to study the relationships between individual pairs of source parameters. The logarithmic seismic moment may be well correlated to the local magnitude, and if its relationship to the other source parameters can also be defined, it becomes possible to convert local magnitude to each of the source parameters via its relationship with the seismic moment. It is then possible to use all 402 recorded events instead of only the 66 events that were analysed successfully in detail. The relationships of seismic moment with local magnitude and the other source parameters, namely fault radius, average coseismic slip and stress drop, were determined using the double-error regression analysis of York (1966). This has the advantage that it assumes errors in both regression variables, rather than the norm of regressing one variable and its error onto another variable that is assumed error-less. This extension is essential because it influences the coefficients of the regression, whereas further refinement is of diminishing statistical importance in comparison.

Paired values of $\log M_0$ with M_L , $\log r$, $\log \Delta\sigma$ and $\log s$ are extracted from Table 4 and illustrated in Figs 13(a)–(d) along with the fitted regression lines. The resulting regression equations and correlation coefficients (r_c) are

$$\log M_0 = 10.71(\pm 0.09) + 0.79(\pm 0.04)M_L \quad r_c = 0.93, \quad (6)$$

$$\log M_0 = 0.6(\pm 1.1) + 6.0(\pm 0.5)\log r \quad r_c = 0.71, \quad (7)$$

$$\log M_0 = 10.7(\pm 0.2) + 1.6(\pm 0.1)\log \Delta\sigma \quad r_c = 0.72, \quad (8)$$

$$\log M_0 = 11.79(\pm 0.05) + 1.38(\pm 0.07)\log s \quad r_c = 0.90. \quad (9)$$

Eq. (6) represents an excellent degree of correlation between the two different estimates of earthquake size. It enables calculation of seismic moment for events with known local magnitude in the area, i.e. all 402 events recorded in Pavliani. This result is consistent with various other studies that find good correlation between seismic moment and local magnitude (e.g. Aki 1967; Archuleta 1986; van Eck & Hofstetter 1989). The resulting gradient is also comparable with that given for California ($\log M_0 = 10 + 1.2 M_L$; Bakun 1984), that calculated for several areas in Greece ($\log M_0 = 10.44 + 0.94 M_L$;

Table 4. Listing of source parameters for 66 of the 70 VOLNET well-located events. No = event number according to the location listing Table 3, M_L = local magnitude given by VOLNET, M_o = seismic moment in $\times 10^{12}$ N m, r = fault radius in m, $\Delta\sigma$ = stress drop in bars, s = slip in mm, No = number of Ω_o readings, Nf = number of f_c readings. The values above and under each calculated parameter are the maximum and minimum respectively, indicating the range within which the value is defined.

No Event	M_L	M_o ($\times 10^{12}$ Nm)	r (m)	$\Delta\sigma$ (bars)	s (mm)	No Ω_o (Ω_o) (f_c)	No Event	M_L	M_o ($\times 10^{12}$ Nm)	r (m)	$\Delta\sigma$ (bars)	s (mm)	No Ω_o (Ω_o) (f_c)
1	3.8	45.4 29.4	156.1 135.0	100.0 52.3	25.12 17.11	5	16	2.2	3.6	107.1 95.2	25.1 13.4	4.61 3.09	5
		19.0	116.7	27.3	11.66			1.9	84.5	7.2		2.08	4
2	2.0	4.6 2.8	107.3 105.8	13.2 10.2	3.18 2.63	5	17	2.2	4.9	102.7 97.3	22.9 16.8	4.86 3.96	6
		1.7	104.3	7.9	2.17			2.6	92.2	12.3		3.24	4
3	2.3	4.4 2.5	113.3 101.3	20.0 10.6	3.94 2.60	6	18	2.9	8.8	124.2 111.8	46.2 27.7	10.28 7.50	8
		1.4	90.5	5.6	1.71			6.5	100.6	16.6		5.47	7
4	1.9	3.3 2.2	109.8 102.9	13.0 8.7	2.84 2.18	7	19	2.4	4.8	126.4 113.9	24.3 14.3	5.49 3.95	7
		1.4	96.4	5.9	1.68			3.8	102.6	8.5		2.85	6
5	2.6	4.5 2.9	180.3 137.1	30.2 7.6	5.93 2.54	7	20	2.3	2.9	148.2 118.5	24.1 7.6	4.49 2.18	6
		2.9	104.2	1.9	1.08			2.0	94.8	2.4		1.05	4
6	2.6	8.9 6.6	108.4 105.3	30.0 24.8	7.21 6.35	4	21	2.8	7.8	156.9 114.8	112.7 22.7	17.30 6.31	8
		5.0	102.3	20.6	5.58			2.0	83.9	4.6		2.30	7
7	2.5	10.6 8.2	130.3 115.5	41.6 23.2	9.29 6.50	8	22	3.0	12.6	137.4 118.4	68.0 33.3	14.80 9.57	8
		6.3	102.3	12.9	4.55			7.7	102.0	16.3		6.19	7
8	2.6	15.9 9.4	136.3 112.0	75.1 29.2	14.15 7.93	7	23	2.6	6.6	134.0 125.7	20.9 14.5	5.60 4.43	6
		5.5	92.1	11.3	4.44			4.4	117.8	10.1		3.50	5
9	2.3	5.3 4.2	106.9 103.8	19.6 16.3	4.65 4.11	7	24	2.3	4.3	110.5 105.4	13.9 9.9	3.20 2.52	6
		3.3	100.8	13.6	3.63			1.6	100.5	7.0		1.99	4
10	2.4	6.1 4.5	128.6 114.1	24.4 13.2	5.36 3.66	7	25	2.2	2.8	112.8 101.5	21.0 11.6	4.21 2.85	4
		3.3	101.1	7.2	2.50			1.6	91.4	6.4		1.93	3
11	2.4	4.6 3.8	117.2 108.2	20.0 13.3	4.51 3.49	6	26	3.0	11.8	153.3 126.8	61.5 25.4	13.31 7.80	9
		3.2	99.8	8.8	2.69			8.5	104.9	10.5		4.57	8
12	2.7	5.8 3.9	135.1 117.8	21.2 10.4	4.64 2.97	5	27	2.0	3.8	120.2 110.4	20.2 12.4	4.58 3.31	6
		2.6	102.7	5.1	1.90			2.2	101.5	7.6		2.40	5
13	2.2	3.8 2.3	109.6 96.3	22.8 11.1	4.14 2.60	6	28	2.5	7.4	129.1 111.1	35.1 16.6	7.12 4.47	6
		1.4	84.6	5.4	1.63			3.7	95.6	7.8		2.80	5
14	2.3	3.5 2.4	105.6 90.2	33.7 14.6	5.43 3.19	6	29	2.9	12.6	116.2 100.3	109.3 54.4	20.31 13.25	9
		1.7	77.0	6.3	1.87			7.8	86.6	27.1		8.65	7
15	2.3	5.2 3.6	127.4 96.4	72.3 17.7	9.96 4.13	6	30	1.8	1.6	100.8 85.9	26.6 10.9	4.05 2.27	6
		2.5	73.0	4.3	1.72			1.0	73.2	4.5		1.28	3

Table 4. (continued.)

NO Event	MO ($\times 10^{12}$ Nm)	\bar{r} (m)	$\Delta\sigma$ (bars)	\bar{b} (mm)	NO (ξ_c)	NO (ξ_c)	NO Event	MO ($\times 10^{12}$ Nm)	\bar{r} (m)	$\Delta\sigma$ (bars)	\bar{b} (mm)	NO (ξ_c)	NO (ξ_c)
31	2.3	3.7	120.9	10.0	2.43	6	49	2.2	6.6	132.0	49.5	7.72	4
	1.4	1.4	113.7	6.7	1.85	6		3.5	103.2	13.8	3.45	1.54	3
			107.0	4.5	1.41	6		1.8	80.6	3.8			
32	2.3	3.1	102.9	19.2	3.78	6	50	3.4	50.9	166.9	298.2	59.65	8
	2.4	1.9	94.9	8.0	2.17	6		28.3	129.3	102.9	35.5	17.47	8
			87.5	8.0	2.17	6			100.2	35.5			
33	2.5	8.6	127.2	25.9	5.98	7	51	2.9	16.4	117.0	77.4	18.13	6
	5.3	3.3	115.2	15.2	4.25	7		10.2	109.6	54.6	14.51	11.61	7
			104.4	8.9	3.03	7		7.1	132.9	33.4	6.53	5	4
34	2.6	9.3	137.0	28.2	6.82	7	52	2.5	4.5	111.9	13.9	5.8	5
	5.1	5.1	122.8	16.4	3.48	7		2.8	84.3	25.5	4.46	5	2
			110.0	9.5	2.64	6		1.6	75.9	13.8	2.97	2	2
35	2.2	3.2	107.8	18.1	3.62	6	53	2.1	2.2	80.0	18.8	3.64	5
	2.4	1.8	98.4	11.1	1.93	6		1.6	105.6	17.1	3.31	5	2
			89.8	6.8	1.93	5		1.4	87.5	6.0	1.68	5	2
36	2.2	5.6	107.9	14.2	3.47	5	54	2.0	2.1	96.1	10.1	2.36	5
	3.0	1.6	107.9	7.9	2.21	5		4.5	107.0	17.0	3.73	5	3
			107.9	7.9	2.21	9		2.8	101.3	11.9	2.93	2.30	3
37	3.3	25.4	134.5	46.7	12.75	9	55	2.1	7.8	123.9	61.3	9.50	7
	15.5	14.9	126.7	33.3	10.24	9		4.2	88.6	19.0	5.9	2.18	6
			113.2	12.4	4.76	7		2.2	78.5	5.9			6
38	3.0	10.3	142.9	38.5	9.55	7	56	2.7	7.8	123.9	61.3	9.50	7
	7.1	7.1	127.2	21.9	4.76	6		4.2	329.2	197.8	53.44	4	4
			113.2	12.4	4.76	6		2.2	225.9	36.0	19.74	7.29	4
39	2.5	9.1	110.5	29.0	6.81	6	58	4.2	12.5	155.0	6.6	6.6	4
	5.9	3.9	105.9	21.9	5.63	6		4.8	11.6	236.9	35.4	6.54	2
			101.4	16.6	4.66	8		2.0	161.1	5.0	1.95	.58	2
40	2.7	11.1	126.2	37.3	8.67	8	59	2.3	4.8	109.5	.7		2
	8.0	5.8	114.7	23.2	4.81	8		2.0	109.5	.7			2
			104.2	14.4	4.81	7		6.1	100.2	25.4	5.27	4	3
41	2.1	3.1	114.6	43.7	5.85	7	60	2.3	3.5	95.3	17.8	4.12	4
	1.9	1.1	89.4	11.5	2.50	7		2.0	90.6	12.5	3.22	4	3
			69.7	3.0	1.07	3		2.0	218.4	22.9	8.15	7	6
42	2.2	3.3	135.8	30.3	4.89	6	61	3.0	18.8	190.3	12.0	6.2	6
	1.7	1.7	106.5	8.5	2.4	6		12.3	165.7	6.2	3.74	6	6
			83.5	2.4	.99	3		28.9	218.4	22.9	8.15	7	6
43	3.0	13.2	99.0	63.9	13.39	8	64	2.3	3.0	87.2	19.9	4.20	2
	9.6	6.9	94.5	49.6	11.37	8		.9	66.4	4.5	1.60	2	2
			90.2	38.5	9.66	8		11.0	101.3	98.2	14.84	6	4
44	2.7	8.1	108.4	51.2	9.19	6	65	2.4	6.0	85.5	41.7	8.65	6
	5.1	3.2	95.0	26.0	6.00	6		3.2	72.2	17.7	5.04	4	4
			83.2	13.2	3.91	5		4.6	115.0	40.4	7.29	4	4
45	2.9	11.0	174.0	29.0	6.68	8	66	2.6	4.2	98.9	19.1	4.59	4
	6.6	4.0	141.2	10.3	3.53	8		3.9	85.1	9.0	2.88	4	4
			114.5	3.7	1.87	7		5.6	107.0	22.5	4.96	3	3
46	2.6	10.7	104.7	61.9	11.71	8	67	2.4	3.9	101.3	16.3	4.00	3
	7.1	4.7	94.5	36.9	8.46	8		2.6	95.8	11.7	3.22	3	3
			85.3	22.0	6.11	7		5.0	97.7	47.6	7.17	3	3
47	2.1	4.4	98.8	22.8	4.70	6	68	2.0	2.7	83.7	20.5	4.17	3
	3.2	2.4	93.9	17.0	3.88	6		1.5	71.6	8.9	2.42	3	3
			89.3	12.7	3.20	4		2.6	127.2	27.4	4.65	3	2
48	1.8	.9	65.4	18.5	2.70	4	69	2.2	2.4	103.8	9.6	2.41	3
	.7	.7	62.7	10.7	1.85	2		2.3	84.7	3.3	1.24	2	2
			10.7	1.85	1.85	4		2.3	84.7	3.3	1.24	2	2

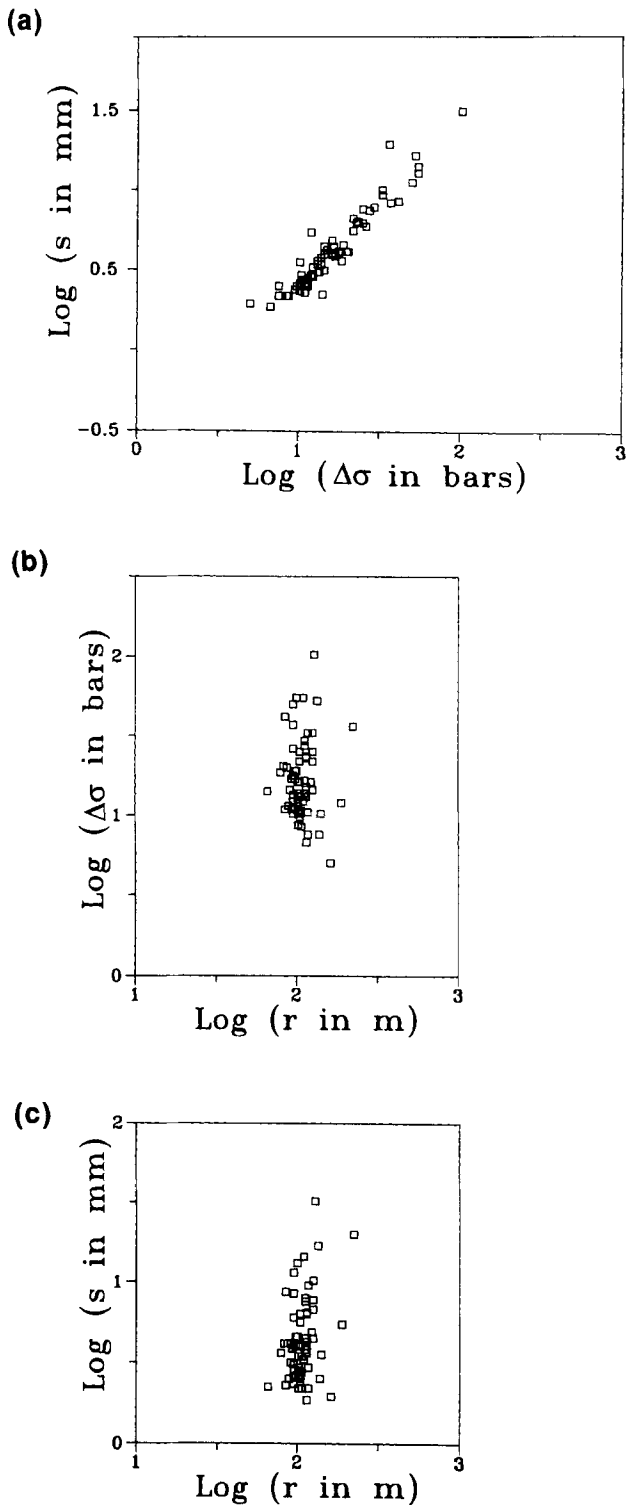


Figure 12. Relationships between seismotectonic source parameters in Pavliani: (a) average slip, s , and average stress drop, $\Delta\sigma$; (b) average stress drop, $\Delta\sigma$, and fault radius, r ; and (c) average slip, s , and fault radius, r .

Abercrombie 1991) and that for the Volos area, Greece ($\log M_0 = 10.1 + 0.96M_L$; Burton *et al.* 1991).

Although source radius varies only slightly over a wide range of seismic moments, as well as over stress drops and average coseismic slips (see Fig. 12), its correlation coefficient of 0.71 with seismic moment is fairly good (see Fig. 13b). So although the correlation between seismic moment and fault radius is poorer than the $\log M_0:M_L$ correlation, eqs (6) and (7) allow fault radius to be assessed for any event of known local magnitude in the Pavliani area. The regression with stress drop (eq. 8) produces a similar degree of correlation. However, the scaling between seismic moment and stress drop which exists for these low-seismic-moment events should be noted. This is well demonstrated for the Pavliani area and is consistent with other studies (again, Aki 1967; Archuleta 1986; van Eck & Hofstetter 1989), which show that stress drop is not constant after passing a lower bound value of seismic moment approximately equal to 10^{14} N m.

Both regression equations (6) and (9) have correlation coefficients of 0.9 or greater, and so the estimates of average slip from M_L will be more reliable than either stress drop or fault radius from M_L . Using all four equations allows the source parameters of any event of known local magnitude to be estimated by relating the local magnitude to the seismic moment and then estimating fault radius, stress drop and seismic slip. These accumulated source parameters will now be investigated in order to study the overall coseismic crustal deformation of the Pavliani fault zone.

3.4 Coseismic deformation and cumulative average coseismic slip distributed within the Pavliani fault zone

Applying eq. (6) to each local magnitude allows estimation of seismic moment for all 402 events. Taking into account that the period of continuous recording in Pavliani was approximately two years, the seismic moment release rate can be calculated for the magnitude range 1–4.6 M_L and contoured spatially over the area. The area defined by the seismicity in Fig. 5 was divided into cells with dimensions of 2.5 km by 2.5 km, and the sum of individual seismic moments calculated for each cell. The resulting values were halved, because they refer to the two year recording period. Fig. 14 shows the seismic moment release rate in 10^{12} N m yr^{-1} contoured over the fault zone. It identifies two areas of relatively high seismic moment release rate, one in the east of the zone and one in the centre. Most of the epicentres represented in Fig. 14 are constrained within a fairly narrow band of approximate width 5 km at the surface of the Earth.

As shown in Figs 5–6, the Pavliani seismicity defines an approximately *vertical* fault zone trending WSW–ENE and extending to about 25 km depth. It is appropriate to examine seismic moment release rate and the seismotectonic source parameters in the fault plane. Fig. 15(a) shows seismic moment release rates projected in the fault plane, highlighting the peaks in the central and the eastern parts of the zone, but resolving more detail. The eastern peak is the slightly higher of the two, reaching about $150\text{--}165 \times 10^{12}$ N m yr^{-1} compared with $135\text{--}150 \times 10^{12}$ N m yr^{-1} . It is also slightly shallower at about 8 km and is dominated by a very small number of relatively high-seismic-moment events. It should be borne in mind that these seismic moment release rates are calculated over a two year period, whereas most of the activity was confined to two

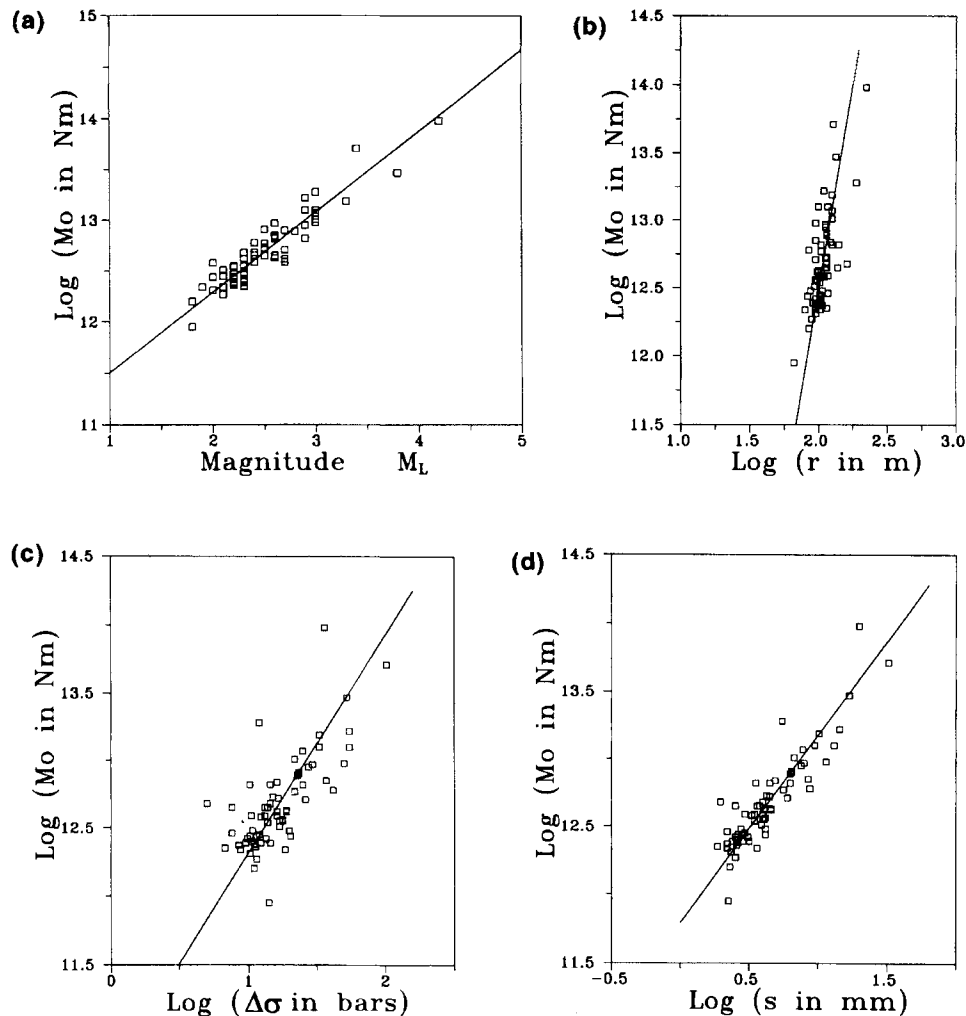


Figure 13. Correlation between seismic moment, M_0 , and earthquake source properties in Pavliani: correlation with (a) local magnitude, M_L , (b) source radius, r , (c) average stress drop, $\Delta\sigma$, and (d) average slip, s . Equations of the regression lines and correlation coefficients are given in the text.

swarms of about one month duration each (Fig. 7a). The moment release rates during these active periods are probably about a factor of 10 higher than those shown in Fig. 15a.

In a similar manner, the seismotectonic parameters of source radius, stress drop and average coseismic slip can be calculated for all the events, and their geometric mean values contoured on the fault plane defined by Figs 5–6. For example, the fault radius is calculated for each of the 402 events using eqs (6) and (7). Then, referring to the previously defined cells, the geometric mean value of source radius is calculated for each cell, enabling contouring of source radius for the whole zone. The averaging process is reasonable because the 2.5 km cell size is considerably larger than the dimension of any of the faults. Fig. 15(b) demonstrates well that the geometrical size of events is relatively large in the eastern part, whereas small events occur throughout the zone.

Eqs (6) and (8) allow the same process to be carried out for stress drops, enabling contouring of stress drop through the whole zone (Fig. 15c). Similarly, eqs (6) and (9) allow calculation and contouring of the average local coseismic slip

(Fig. 15d). The final extension, which is appropriate for slip but not the other seismotectonic parameters, is the calculation of local cumulative slip. Cumulative slip is taken as the scalar sum of slips in an arbitrarily defined area of the fault zone. Hence, the sum of individual slips was calculated for each previously defined cell and Fig. 15(e) is the result.

A comprehensive picture of the fault zone is provided by Figs 15(a)–(e). They highlight that the area of highest seismicity (and high seismic moment release rate) in the central part of the zone corresponds to a peak of cumulative slip. Although the eastern part is characterized by low seismicity, the cumulative slip reaches a local, albeit lower, peak in that part too. This result is due to the influence of two larger events with local magnitude greater than $4 M_L$, and the peak would be higher if a third event of local magnitude $4 M_L$ were included. This event is not given in the Volos network catalogue but is included in the Makropoulos *et al.* (1989) macroseismicity catalogue and should be borne in mind.

The large number of small magnitude events is more than equivalent to the small number of large magnitude events in

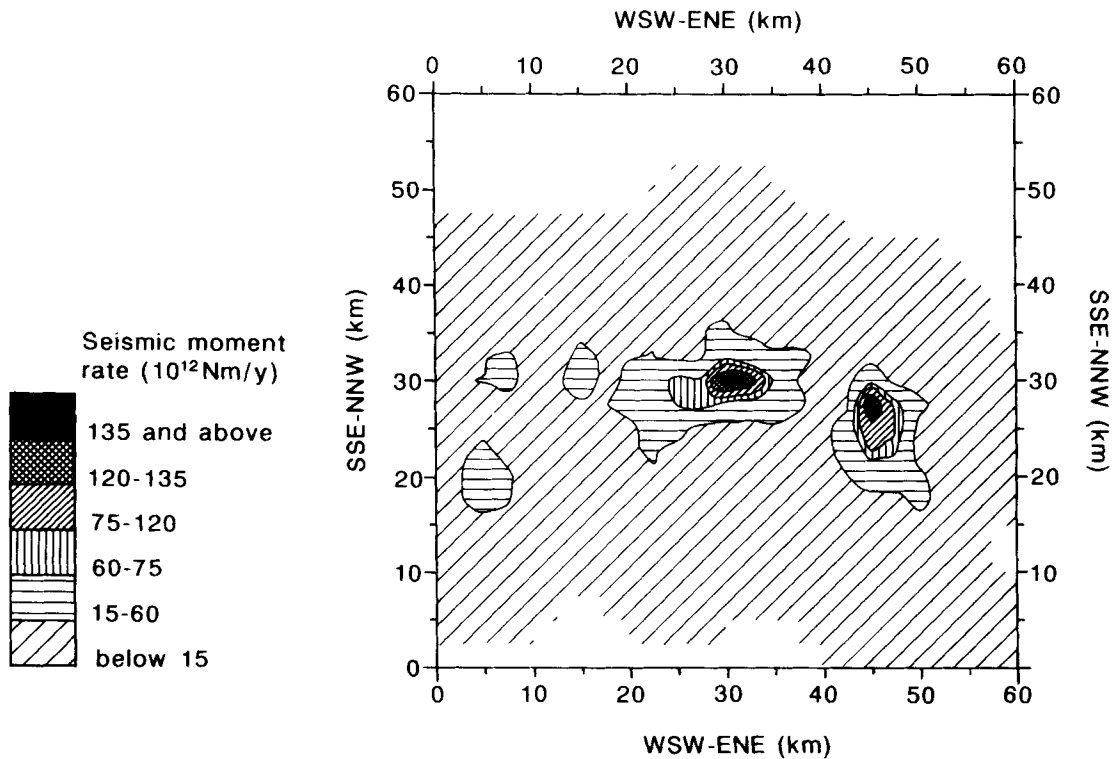


Figure 14. Seismic moment release rate contoured in Pavliani.

terms of cumulative slip. Moreover, a similar interpretation can be given if the seismic moment release rate map is taken into account. This shows that a peak observed in terms of cumulative slip and seismic moment release rate is reached by both a small number of large-magnitude events and a large number of small-magnitude events. Relatively high stress drop occurs in the eastern part only, and relatively low stress drop throughout the rest of the zone.

In view of the above results it is appropriate to explore features of the fault zone that may be recorded in the surface geology. Fig. 16 illustrates the distribution of cumulative coseismic slip mapped on the horizontal plane. The origin in Fig. 16 corresponds to the SW corner of the epicentral maps in Fig. 5 and the area mapped is the result of an anticlockwise rotation towards the direction defined by the line fitted to the mapped epicentres by least squares. The two peaks of cumulative slip are very clear. However, if the distribution of coseismic slip is examined in conjunction with mean stress drop (Fig. 17), a *coincident* occurrence of relatively high cumulative slip and high mean stress drop is observed only for the eastern peak. Furthermore, the eastern peak coexists with a high moment release rate at shallower depths than the central peak, and coseismic deformations may therefore be expected to be less attenuated at the surface. The eastern peak is situated geographically about 7 km east of the village of Kaloscopi (Fig. 18).

Examination of the photogeology stereo pairs and the IGME geological map reveals a mapped 'neotectonic' fault coincident with a major scarp near Kaloscopi. The location of the fault in relation to the seismicity is shown in Fig. 18. Features on this fault were examined in the field by Melis and Brooks. The IGME map shows a 'neotectonic' normal fault downthrown to the north, where a series of alluvial cones have developed.

The scarp face of limestone is deeply weathered and fault-plane lineations possibly associated with recent movement were only found at one locality. Near-vertical zones of friable fault gouge were found behind the main scarp at a few localities, but displacement could not be determined and dating of the gouge is not available. The two largest earthquakes in the Pavliani seismicity have epicentres located only 2 or 3 km north-east of the eastern end (B) of this fault (Fig. 18).

Furthermore, if the Pavliani microearthquake fault zone is treated as a cohesive macro fault plane then Brune's (1968) model can be applied to determine a macro slip rate from the seismic moment release rate. Brune gives the coseismic rate $\langle u \rangle$ as

$$\langle u \rangle = \Sigma M_o / \mu A_o \quad (\text{in mm}), \quad (10)$$

where ΣM_o is the sum of seismic moments from events on a macrofault of area A_o , and μ is the rigidity. This gives an estimate of earthquake slip rate on a fault area which is defined by the seismicity. For our purpose the WSW-ENE zone defined by the microseismicity is taken as a macrofault. The slip will be time-dependent as it represents coseismic slip during the time period over which the data set was collected. The defined fault zone has a length of 60 km and a width of 25 km. The latter equals the maximum focal depth of the seismicity in the area. Still assuming a value of $3 \times 10^{10} \text{ N m}^{-2}$ for the rigidity μ , the total coseismic slip $\langle u \rangle$ for the two year data set is 0.07 mm. Taking into account that the present extensional tectonic regime has existed for at least 5 Ma (Jackson & McKenzie 1988), an estimate for an earthquake displacement equivalent can be calculated. This is estimated to be 175 m, which is similar to the elevation of the major limestone scarp observed south of Kaloscopi.

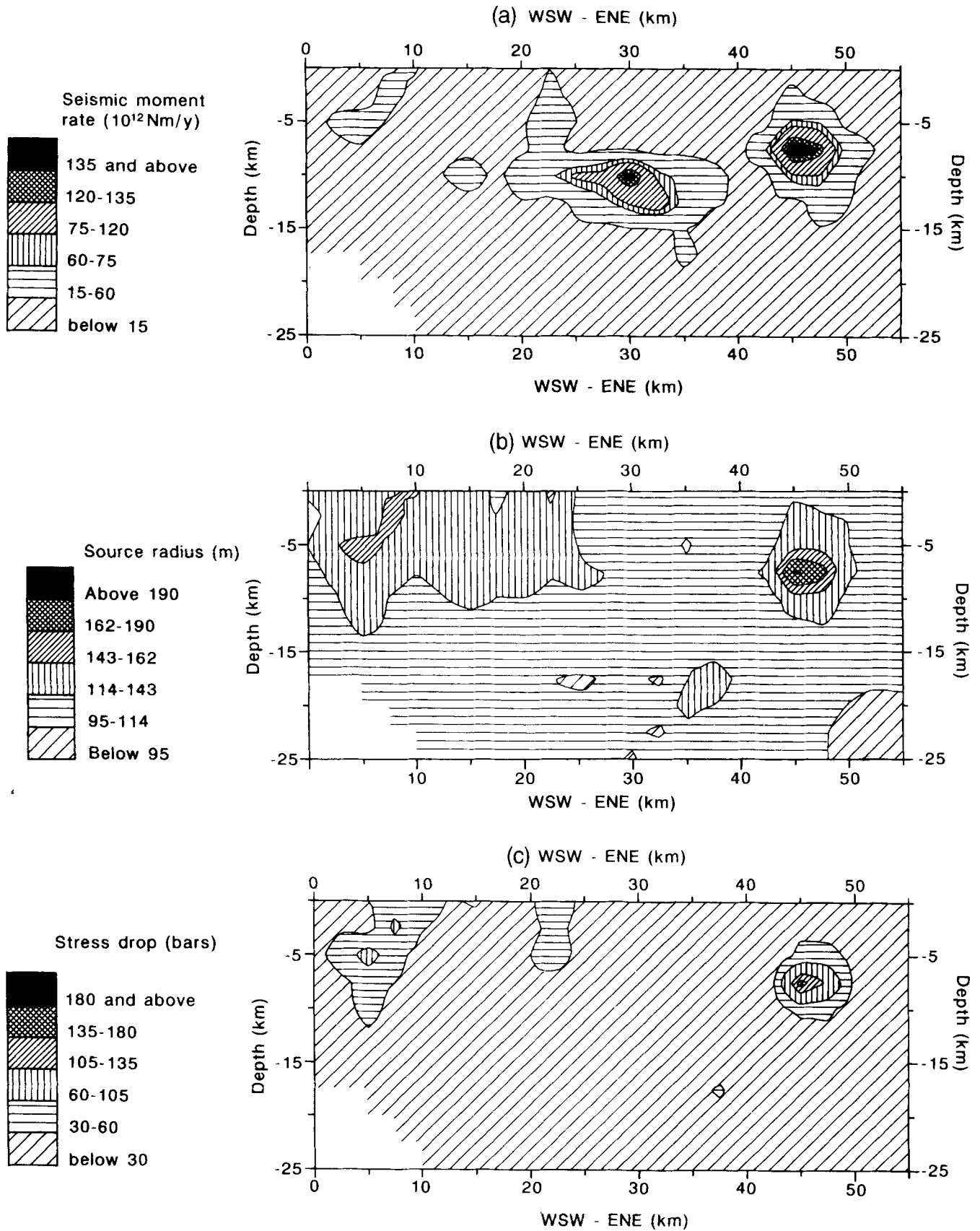


Figure 15. Microearthquake source parameters contoured on the vertical fault plane defined by the epicentral trend line in Fig. 5: (a) seismic moment release rate; (b) geometric mean of source radius; (c) geometric mean of stress drop; (d) geometric mean of coseismic slip; (e) cumulative coseismic slip.

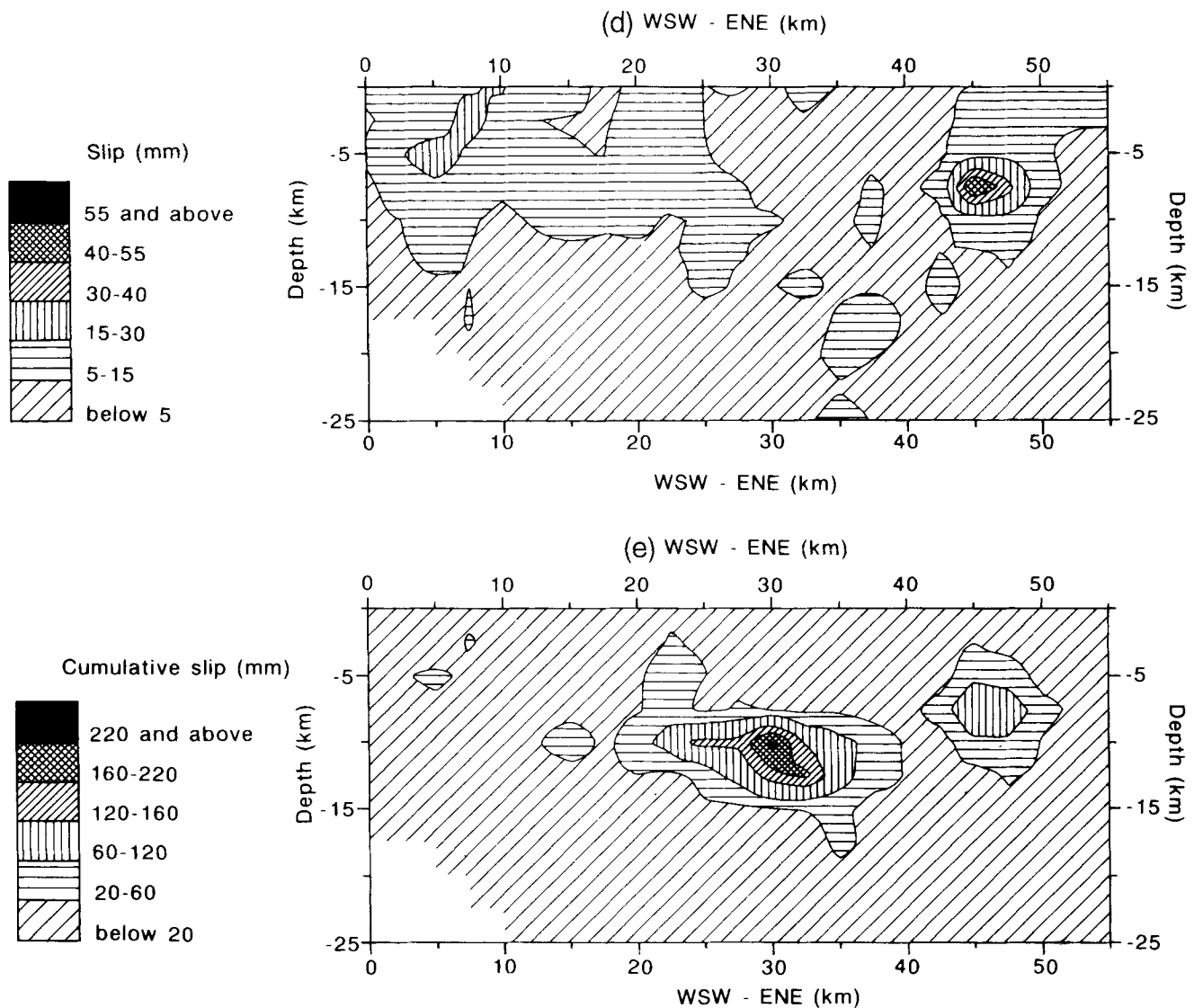


Figure 15. (Continued.)

4 DISCUSSION AND CONCLUSIONS

Although there is no evidence in the historical record of large damaging earthquakes in the Pavliani area since at least 600 BC, it is still an area of high microseismicity. This microseismicity allows examination of the contemporary coseismic crustal deformation in relation to known geological features.

The microearthquakes in the local magnitude range 1–4.6 M_L define an approximately vertical fault zone trending WSW–ENE, of 60 km length and 25 km depth. Temporal variations in the overall microseismicity show two principal periods of swarm activity with negligible migration between them, and the individual microearthquakes are well distributed throughout the zone. The largest earthquake observed, 4.6 M_L , produces a reasonably well constrained fault-plane solution. This shows a strike direction consistent with the trend of the microseismicity zone, and an extension direction consistent with many large earthquakes ($>5.5 M_s$) in central Greece associated with the extensional Aegean domain.

The large number of recorded microearthquakes lends itself to examination of seismotectonic parameters throughout the

fault zone. Extensive investigations to define conventions or criteria to assist with spectral analysis produced two guidelines. First, it was found preferable to define the P window used for spectral analysis by encapsulating the longest possible P coda that is not disturbed by other phases. Secondly, the main criterion for applying a Q -correction was found to be determined simply by the hypocentral distance to the recording station. Site effects were minimized by using seismometer emplacements in hard basement rock. The Q -correction became important at distances greater than 40 km, although the results do not vary considerably.

The final seismotectonic source parameters were determined using spectral analysis of the P wave obtained by selective windowing designed to exclude other P phases from the coda. Using only well-located earthquakes, we obtain seismic moments in the range $1\text{--}95 \times 10^{12}$ N m, source radii of 65–226 m, average stress drops of 5–103 bars and average coseismic slips of 2–32 mm. The source radii vary slowly but systematically over the range of seismic moments, but the scatter in the data indicates that faults of similar geometrical size can produce relatively low as well as relatively high stress

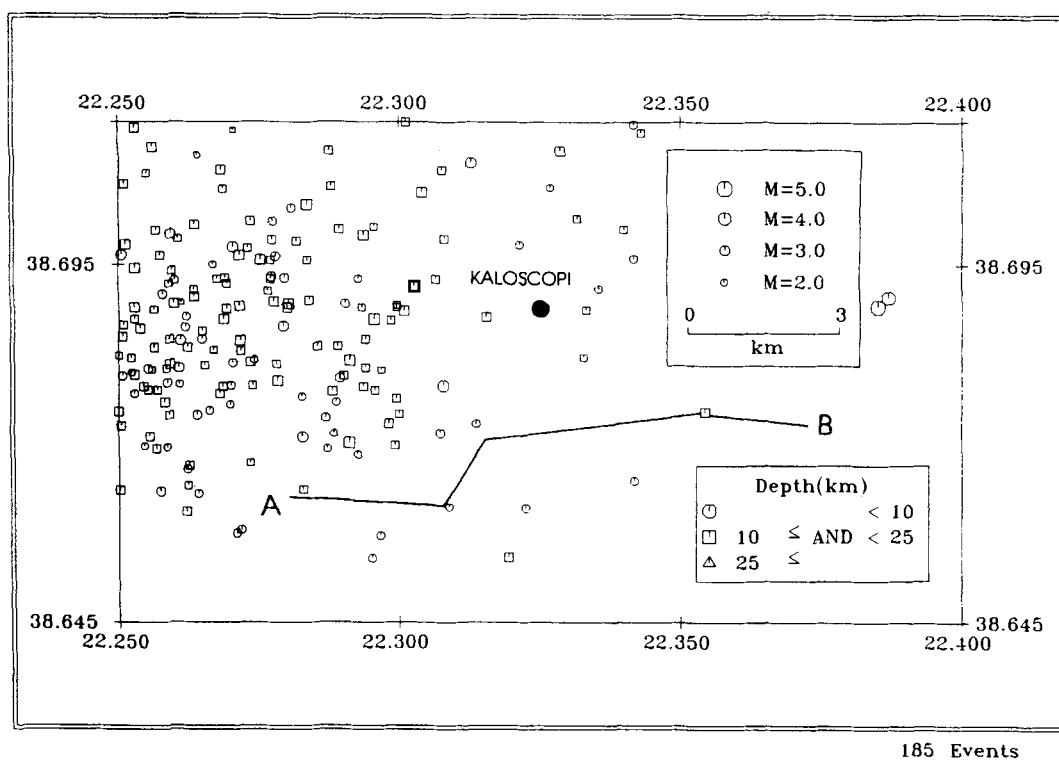


Figure 18. Epicentres of microearthquakes located near Kaloscopi village, and the fault mapped 2 km south of Kaloscopi. Local magnitudes, M_L , are plotted.

drop and slip events. The relatively slow variation of source radius has been noted elsewhere by, for example, Burton *et al.* (1991) and Abercrombie & Leary (1993), and in the latter case extending over six degrees of magnitude (spanning mining tremors to large earthquakes), suggesting self-similarity and scaling over a wide range. However, at this time it is difficult to make all observations of the associated stress drops accord simply with a constant stress drop because of (a) uncertainties in the observations and (b) clear observational and theoretical indications that it should not be a constant in all tectonic regimes and frictionally influenced stress fields (Sibson 1974; Kanamori & Anderson 1975; Burton 1993).

Of prime utility in mapping coseismic deformation is the excellent correlation found for seismic moment with magnitude, and also with average coseismic slip (correlations with source radii and stress drop are poorer). Various authors similarly find good correlation for seismic moment with magnitude (e.g. Aki 1967; Bakun 1984; Archuleta 1986; van Eck & Hofstetter 1989; Burton *et al.* 1991; Abercrombie 1991), and in our case this allows heterogeneity in the distribution of seismotectonic parameters to be mapped onto the vertical fault-zone plane for the whole set of microearthquakes (402 events) recorded during 1983–84 rather than just for the sample (66 events) used for best determination of these parameters and correlations.

Extension to the whole set of microearthquakes allows mapping of parameters representative of the coseismic deformation history during 1983–84: thus cumulative coseismic slip and seismic moment release rate are mapped. Peaks of high moment release rate occur in the east and centre of the fault zone. That in the east is dominated by a few large-moment-release events which are also relatively large geometrically,

whereas the peak in the centre is produced by a large number of small events. Both moment release rate peaks, despite their locally different component seismicity, are associated with locally high cumulative coseismic slip.

Only the eastern peak is also associated with high stress drop. It is also shallower, and therefore any surficial interaction is likely to be less attenuated. The surface projection of this peak is geographically within 3 km of a mapped normal fault coincident with an Alpine thrust front delineated by a major scarp. Evidence of recent movement on this fault at the surface is only slight. Friable fault gouge is seen at a few localities, but dating of the fault gouge is not available to determine if it is of neotectonic age. However, considering the whole fault zone as a cohesive entity and using a Brune estimate of slip at the current moment release rate throughout the present extensional tectonic regime suggests a total vertical displacement of about 175 m, similar to the elevation of the scarp.

Overall, these observations support the possibility of a surface break in the Pavliani area, particularly in the Kaloscopi district. However, neotectonic displacements at the surface immediately above the zone of seismicity may be minimal for two reasons. First, if the local seismicity existing below 7 km involves significant crustal displacements, as expected, these displacements may be markedly attenuated in the uppermost part of the crust. Second, the zone of active faulting at the surface may be significantly offset from the zone of seismicity at depth. However, reconnaissance of a broad zone during the detailed study of the Kaloscopi district revealed no alternative neotectonic fault lines. The higher stress drops associated with the eastern end of the fault zone may also be indicative of the fracture tip progressing in the segment of the fault located in this district.

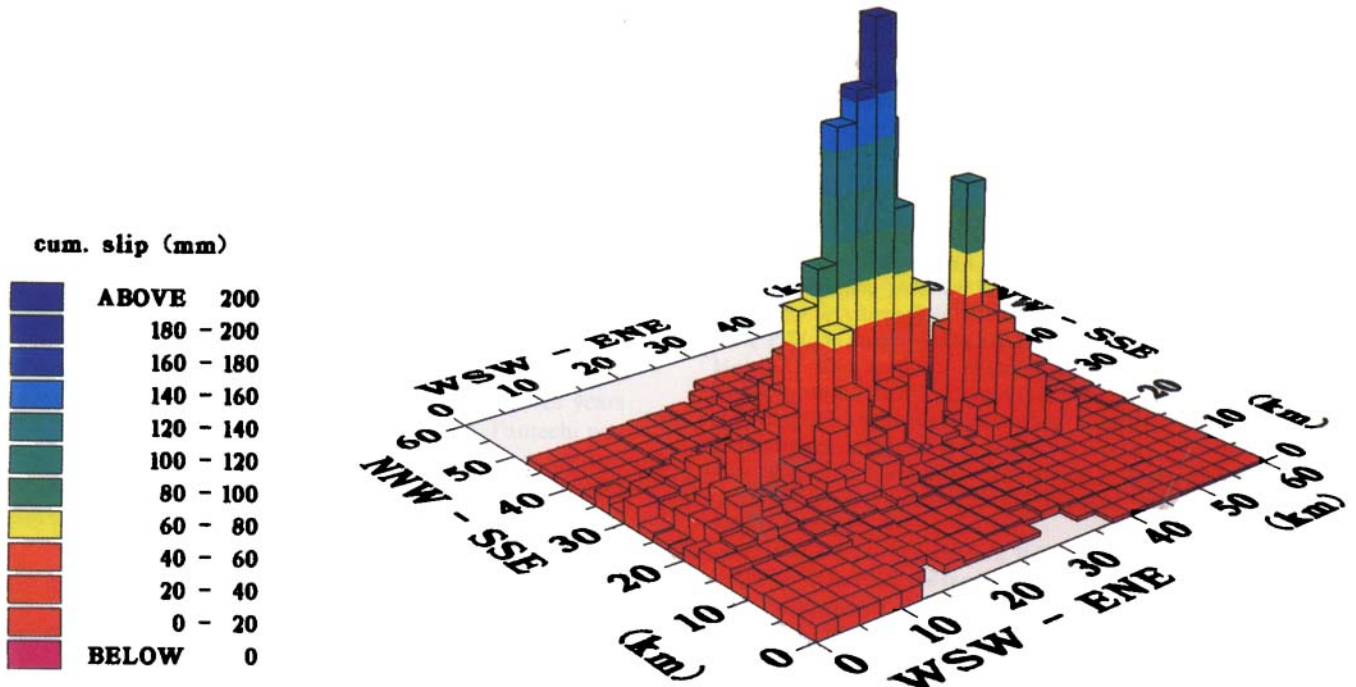


Figure 16. Distribution of cumulative coseismic slip in the Pavliani area.

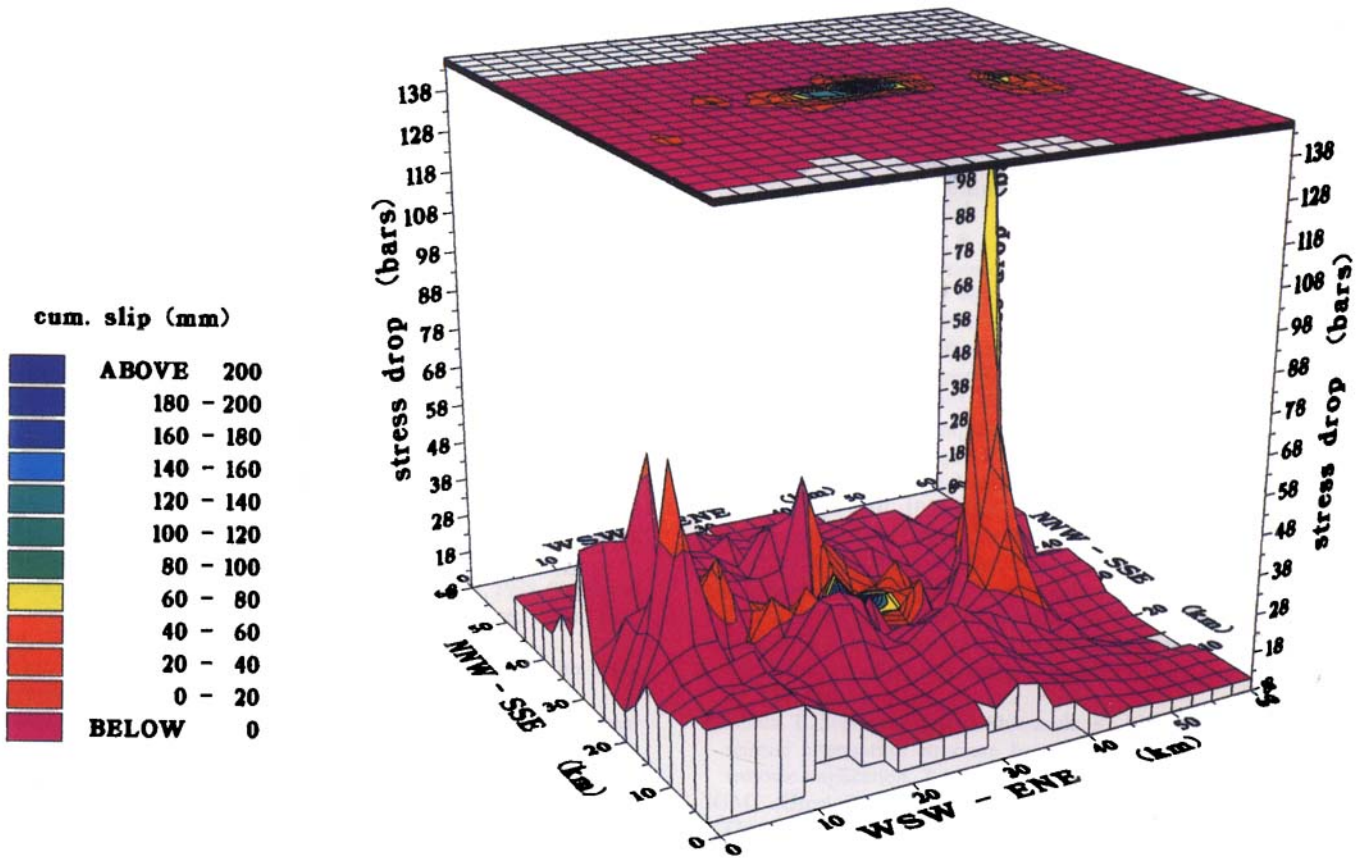


Figure 17. 3-D representation of the distribution of stress drop and superimposed contour map of cumulative coseismic slip in Pavliani.

ACKNOWLEDGMENTS

The Patras seismic network was supported by the Universities of Cardiff and Patras, and the Volos seismic network by the British Geological Survey and the University of Athens, including support from the Natural Environment Research Council and assistance with data transmission from the British Embassy. People too numerous to mention have helped with these networks, both at villages in the field and in the laboratory, and they should know that we are glad to have had their generous help. One of us (NSM) must also thank the University of Wales for a scholarship, and the Directorate General for Science, Research and Development of the European Communities for generous financial support over three years (EC Sectoral Grant B/86000071) in which Dr R. Fantechi was instrumental. Continuing support for part of this work was provided by NERC Grant GR9/1005 and now by NATO Collaborative Research Grant 9407180.

REFERENCES

- Abercrombie, R.E., 1991. Earthquake rupture dynamics and neotectonics in the Aegean region, *PhD thesis*, University of Reading.
- Abercrombie, R. & Leary, P., 1993. Source parameters of small earthquakes recorded at 2.5 km depth, Cajon Pass, Southern California: implications for earthquake scaling, *Geophys. Res. Lett.*, **20**, 1511–1514.
- Aki, K., 1967. Scaling law of seismic spectrum, *J. Geophys. Res.*, **84**, 6140–6148.
- Ambraseys, N.N. & Jackson, J.A., 1990. Seismicity and associated strain of central Greece between 1890 and 1988, *Geophys. J. Int.*, **101**, 663–708.
- Anderson, J.G., 1986. Implication of attenuation for studies of the earthquake source, *Earthquake Source Mechanics, AGU Monograph*, **37**, 311–318.
- Archuleta, R.J., 1986. Downhole recordings of seismic radiation. *Earthquake Source Mechanics, AGU Monograph*, **37**, 319–329.
- Archuleta, R.J., Cranswick, E., Mueller, C. & Spudich, P., 1982. Source parameters of the 1980 Mammoth Lakes, California, earthquake sequence, *J. Geophys. Res.*, **87**, 4595–4607.
- Aster, R.C. & Shearer, P.M., 1991. High-frequency borehole seismograms recorded in the San Jacinto fault zone, southern California, *Bull. seism. Soc. Am.*, **81**, 1081–1100.
- Bakun, W.H., 1984. Seismic moments, local magnitudes, and coda-duration magnitudes for earthquakes in central California, *Bull. seism. Soc. Am.*, **74**, 439–458.
- Bath, M., 1983. The seismology of Greece, *Tectonophysics*, **98**, 165–208.
- Brooks, M. & Ferentinos, G., 1984. Tectonics and sedimentation in the Gulf of Corinth and the Zakynthos and Kefallinia Channels, western Greece, *Tectonophysics*, **101**, 25–54.
- Brooks, M., Clews, J.E., Melis, N.S. & Underhill, J.R., 1988. Structural development of Neogene basins in western Greece, *Basin Res.*, **1**, 129–138.
- Brune, J.N., 1968. Seismic moment, seismicity, and rate of slip along major fault zones, *J. Geophys. Res.*, **73**, 777–784.
- Brune, J.N., 1970. Tectonic stress and the spectra of seismic shear waves from earthquakes, *J. Geophys. Res.*, **75**, 4997–5009.
- Brune, J.N., 1971. Correction, *J. Geophys. Res.*, **76**, 5002.
- Brune, J.N., Fletcher, J.B., Vernon, F.L., Haar, L., Hanks, T.C. & Berger, J., 1986. Low stress-drop earthquakes in the light of new data from the Anza, California telemetered digital array, *Earthquake Source Mechanics, AGU Monograph*, **37**, 237–245.
- Burton, P.W., 1993. Microearthquakes and efficiency in crustal deformation in Greece, in *Proc. 2nd Congress Hellenic Geophys. Un. Meet.*, pp. 11–38, eds Papazachos, B.C., Papadimitriou, E., Tsaparas, Th., Tsokas, G., Vlahov, D. & Konstantinidow, E., Piziti, Thessaloniki.
- Burton, P.W. & Blamey, C., 1972. A computer program to determine the spectrum and a dispersion characteristic of a transient signal, UKAEA AWRE Report No O48/72, HMSO.
- Burton, P.W. & Marrow, P.C., 1989. Seismic hazard and earthquake source parameters in the North Sea, in *Earthquakes at North-Atlantic Passive Margins: Neotectonics and Postglacial rebound, NATO Series C: Mathematical and Physical Sciences*, vol. 266, pp. 633–664, Kluwer Academic Publishers, Dordrecht.
- Burton, P.W., McGonigle, R.W., Ritchie, M.E.A., Raines, M.G., Morgan, S.N., Makropoulos, K.C. & Agelis, S., 1983–84. *VOLNET Station Bulletins, Jan 1983–Dec 1984*, Brit. Geol. Surv. and University of Athens, Joint Open File Reports.
- Burton, P.W., Makropoulos, K.C., McGonigle, R.W., Ritchie, M.E.A., Main, I.G., Kouskouna, V. & Drakopoulos, J., 1991. Contemporary seismicity on the Nea Ankhialos fault, eastern Greece: fault parameters of major and minor earthquakes. *Technical Report WL/91/29, Seismology Series*, Brit. Geol. Surv., Edinburgh.
- Collier, R.E.L.I. & Dart, C.J., 1991. Neogene to Quaternary rifting, sedimentation and uplift in the Corinth Basin, Greece, *J. geol. Soc.*, **148**, 1049–1065.
- Comninakis, P.E. & Papazachos, B.C., 1986. A catalogue of earthquakes in Greece and the surrounding area for the period 1901–1985, *Publ. Geophys. Lab. Univ. Thessaloniki*, No. 1.
- Condon, P.J., 1985. Determination of source parameters and attenuation from seismic spectra of shallow earthquakes in the Northern Aegean Sea, *MSc thesis*, University of Durham, UK.
- Delibasis, N.D., 1982. Seismic wave attenuation in the upper mantle beneath the Aegean region, *Pure appl. Geophys.*, **120**, 820–839.
- Doutsos, T. & Piper, D.J.W., 1990. Listric faulting, sedimentation and morphological evolution of the Quaternary eastern Corinth rift, Greece: First stages of continental rifting, *Geol. Soc. Am. Bull.*, **102**, 812–829.
- Drakopoulos, J. & Delibasis, N.D., 1982. The focal mechanism of earthquakes in the major area of Greece for the period 1947–1981. *Seis. Lab., Univ. Athens*, No. 2.
- Evans, R., McGonigle, R. & Fyfe, C., 1985. SGMLIB: A library of Fortran routines for accessing the BGS–GSRG database of digital network seismograms, *British Geological Survey, Glob. Seis. Report*, No. 196, Edinburgh.
- Ferentinos, G., Brooks, M. & Doutsos, T., 1985. Quaternary tectonics in the Gulf of Patras, western Greece, *J. Struct. Geol.*, **7**, 713–717.
- Fletcher, J.B., Haar, L.C., Vernon, F.L., Brune, J.N., Hanks, T.C. & Berger, J., 1986. The effects of attenuation on the scaling of source parameters for earthquakes at Anza, California, *Earthquake Source Mechanics, AGU Monograph*, **37**, 331–338.
- Gagnepain-Beyneix, J., 1985. Variation of source parameters of small western Pyrenean earthquakes and their relation to main shock occurrence, *Ann. Geophys.*, **3**, 381–394.
- Galanopoulos, A.G., 1960. A catalogue of shocks with $I_0 \geq VI$ or $M \geq 5$ for the years 1801–1958. *Seis. Lab., Univ. Athens*.
- Galanopoulos, A.G., 1961. A catalogue of shocks with $I_0 \geq VII$ for the years prior to 1800. *Seis. Lab., Univ. Athens*.
- Galanopoulos, A.G., 1981. The damaging shocks and the earthquake potential of Greece, *Ann. geol. Hellen.*, **XXX/2**, 647–724.
- Hanks, T.C. & Wyss, M., 1972. The use of body-wave spectra in the determination of seismic source parameters, *Bull. seism. Soc. Am.*, **62**, 561–589.
- Hashida, T., Stavarakakis, G. & Shimazaki, K., 1988. Three-dimensional seismic attenuation structure beneath the Aegean region and its tectonic implication, *Tectonophysics*, **145**, 43–54.
- IGME (Greek Institute of Geology and Mineral Exploration), 1960. Geological map 1:50 000 sheet; Amfissa. Mapped during 1954, Athens.
- Jackson, J.A. & McKenzie, D.P., 1988. The relationship between plate motions and seismic moment tensors, and the rates of active deformation in the Mediterranean and Middle East, *Geophys. J. Int.*, **93**, 45–73.
- Kanamori, H. & Anderson, D.L., 1975. Theoretical bases of some

- empirical relations in seismology, *Bull. seism. Soc. Am.*, **65**, 1073–1095.
- Keilis-Borok, V.I., 1959. On the estimation of the displacement in an earthquake source and of source dimensions, *Ann. Geofis.*, **12**, 205–214.
- King, G.C.P. *et al.*, 1985. The evolution of the Gulf of Corinth (Greece): an aftershock study of the 1981 earthquakes, *Geophys. J. R. astr. Soc.*, **80**, 677–693.
- MacBeth, C.D. & Burton, P.W., 1987. Single-station attenuation measurements of high-frequency Rayleigh waves in Scotland, *Geophys. J. R. astr. Soc.*, **89**, 757–797.
- McKenzie, D., 1978. Active tectonics of the Alpine-Himalayan belt: the Aegean Sea and surrounding regions, *Geophys. J. R. astr. Soc.*, **55**, 217–254.
- Madariaga, R., 1976. Dynamics of an expanding circular fault, *Bull. seism. Soc. Am.*, **66**, 636–666.
- Makropoulos, K.C. & Burton, P.W., 1981. A catalogue of seismicity in Greece and adjacent areas, *Geophys. J. R. astr. Soc.*, **65**, 741–762.
- Makropoulos, K.C., Drakopoulos, J.K. & Latousakis, J.B., 1989. A revised and extended earthquake catalogue for Greece since 1900, *Geophys. J. Int.*, **98**, 391–394.
- Melis, N.S., 1986. Geophysical studies of the Gulf of Patras region using the Patras Seismic Network, 1983–84, *MSc thesis*, University of Wales, UK.
- Melis, N.S., 1992. Earthquake hazard and crustal deformation in central Greece, *PhD thesis*, University of Wales, UK.
- Melis, N.S., Brooks, M. & Pearce, R.G., 1989. A microearthquake study in the Gulf of Patras region, western Greece, and its seismotectonic interpretation, *Geophys. J. R. Astr. Soc.*, **98**, 515–524.
- Modiano, T. & Hatzfeld, D., 1982. Experimental study of the spectral content for shallow earthquakes, *Bull. seism. Soc. Am.*, **72**, 1739–1758.
- National Observatory of Athens, 1983. *Greek Network Earthquake Bulletin; September 1983*, Athens.
- Papadopoulos, G.A., Kondopoulou, D.P., Leventakis, G.-A. & Pavlides, S.B., 1986. Seismotectonics of the Aegean region, *Tectonophysics*, **124**, 67–84.
- Papazachos, B.C., 1976. Seismic activity along the Saronicos-Corinth-Patras Gulfs, *Mon. Bull. seism. Inst. nat. Obs.*, Athens, 1–16.
- Papazachos, B.C. & Comninakis, L., 1982a. A catalogue of historical earthquakes in Greece and surrounding area, 479 B.C.–1900 A.D., *Publ. Geophys. Lab. Univ. Thessaloniki*, No. 5.
- Papazachos, B.C. & Comninakis, L., 1982b. A catalogue of earthquakes in Greece and surrounding area for the period 1901–1980. *Publ. Geophys. Lab. Univ. Thessaloniki*, No. 6.
- Papazachos, B.C. & Papazachos, C., 1989. *The Earthquakes of Greece*, Ziti, Thessaloniki.
- Papazachos, B.C., Kiratzi, A.A., Hatzidimitriou, P.M. & Rocca, A.C., 1984. Seismic faults in the Aegean area, *Tectonophysics*, **106**, 71–85.
- Richter, C.H., 1958. *Elementary Seismology*, W.H. Freeman, San Francisco.
- Ritsema, A.R., 1974. The earthquake mechanism of the Balkan region. *Netherl. Meteorol. Inst. Sci. Rep.*, **74–4**, 1–36.
- Roberts, S. & Jackson, J., 1991. Active normal faulting in central Greece: an overview. The Geometry of Normal Faults, *Spec. Publ. geol. Soc. Lond.*, **56**, 125–142.
- Shebalin, N., Karnik, V. & Hadzievski, D., 1974. *Balkan Region—Catalogue of Earthquakes*, UNESCO Project Office, Skopje.
- Sibson, R.H., 1974. Frictional constraints on thrust, wrench and normal faults, *Nature*, **249**, 542–544.
- Street, R.L., Herrmann, R.B. & Nuttli, O.W., 1975. Spectral characteristics of the Lg wave generated by Central United States earthquakes, *Geophys. J. R. astr. Soc.*, **41**, 51–63.
- Thatcher, W. & Hanks, T.C., 1973. Source parameters of Southern California earthquakes, *J. Geophys. Res.*, **78**, 8547–8576.
- Trifunac, M.D., 1972. Stress estimates for the San Fernando, California, earthquake of February 9, 1971: Main event and thirteen aftershocks, *Bull. seism. Soc. Am.*, **62**, 721–750.
- Van Eck, T. & Hofstetter, A., 1989. Microearthquake activity in the Dead Sea region, *Geophys. J. Int.*, **99**, 605–620.
- Vita-Finzi, C. & King, G.C.P., 1985. The seismicity, geomorphology and structural evolution of the Corinth area of Greece, *Phil. Trans. R. Soc. Lond.*, **314**, 379–407.
- York, D., 1966. Least squares fitting of a straight line, *Can. J. Phys.*, **44**, 1079–1086.